

Neutron imaging in a broader perspective

Prof. Dr Robert Zboray[1,2], Group leader X-ray imaging

[1]Center for X-ray Analytics, Swiss Federal Laboratories for Materials Science and Technology (Empa)

[2]Center, University of Bern, 3008 Bern, Switzerland

robert.zboray@empa.ch

Central European Training School and Workshop on Neutron Techniques, BNC, Budapest, 4-9 October, 2026

Outline

- Basics of transmission imaging, neutron vs. X-ray
- Neutron interactions
- Neutron sources, beam formation
- Neutron detection
- CT principles
- Alternative imaging modalities, comparison with X-rays
- Applications

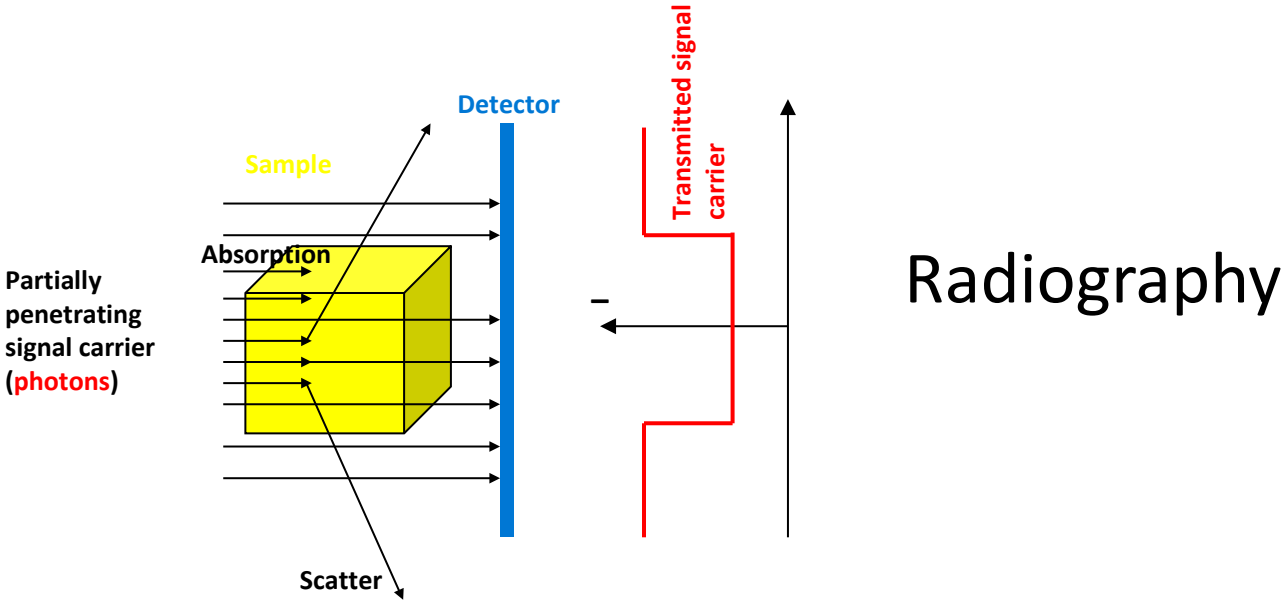
Basics

Radiation-based imaging methods

Transmission imaging:

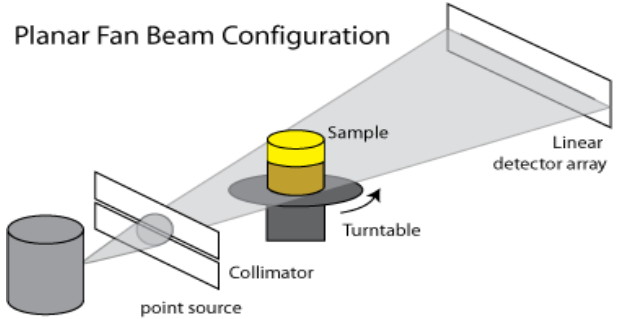
- *X-ray imaging*
- *Gamma imaging*
- *Neutron imaging*

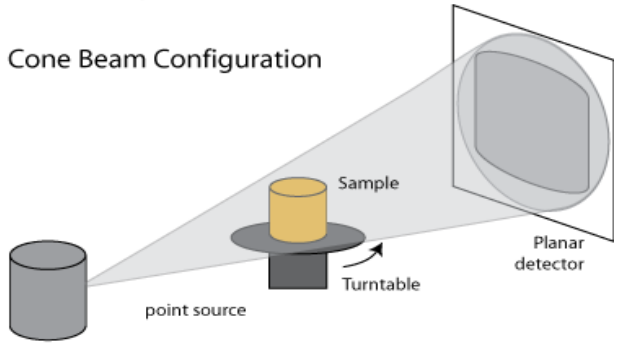
The information on the sample is obtained by the missing signal carriers not reaching the detector (in reference to the case without sample)!

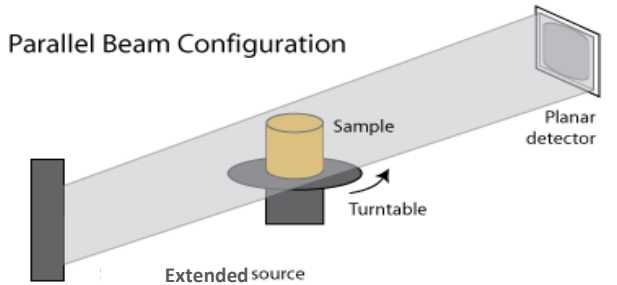


CT principles, geometries

Synchrotronmovies.com







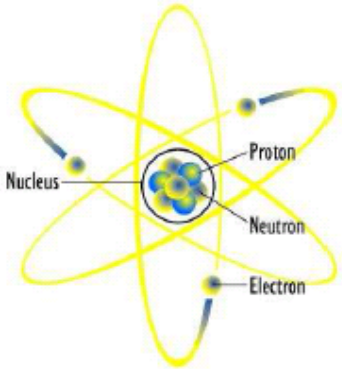
Properties of neutron

Size: $1.6 * 10^{-15}$ m

Mass: $1.674927351(74) * 10^{-27}$ kg

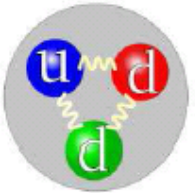
Charge: 0

Spin: ½ (two states possible)



Velocity: few m/s (ultra cold) to speed of light (very fast)

Elementary composition: 3 Quarks up-down-down



Magnetic moment: $-1.913\ \mu_N$

Interaction with matter: nuclear reactions: absorption, scattering, fission

Classification: Baryon, Fermion

Half-life: 881.5 s

Discovered: 1932 by James Chadwick

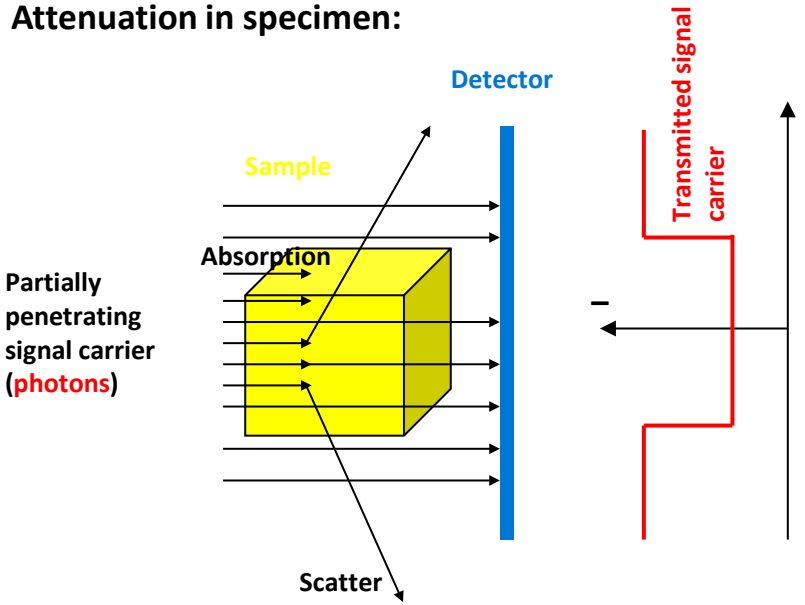
Neutrons vs. X-rays. properties

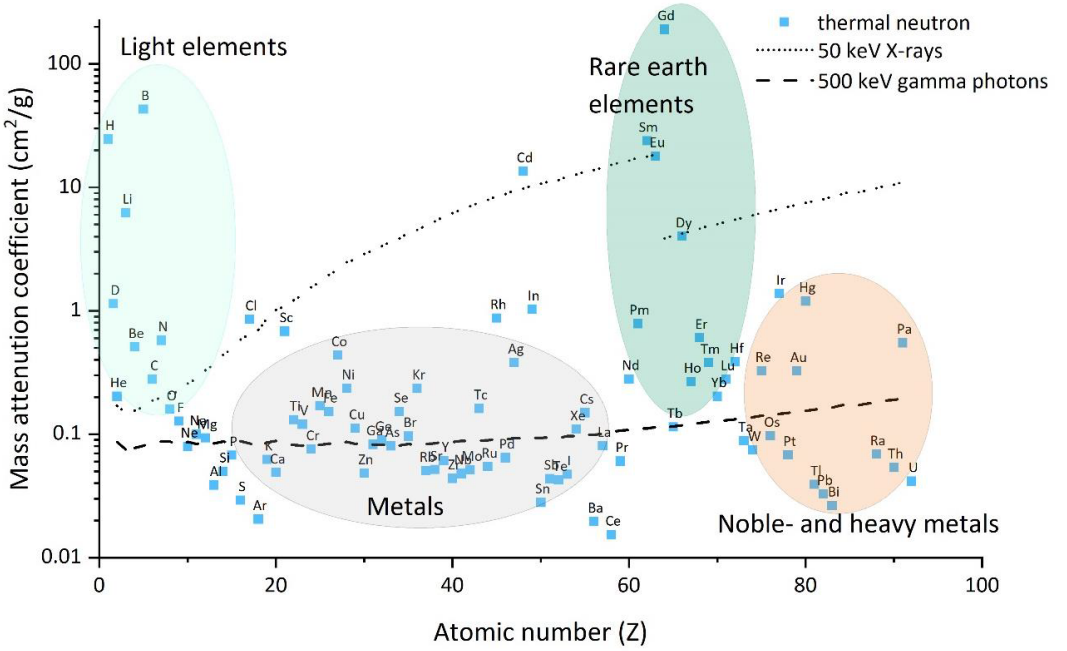
thermal neutrons	X-rays (e.g. 100 keV)
•wavelength: ~ 2 Å = 0.2 nm	•wavelength: 40keV ~ 0.124 A=0.0124nm
•energy: 25 meV	•energy: eV to MeV (E=h*c/λ)
•mass: $1.674927351(74) \cdot 10^{-27}$ kg	•mass: no
•charge: no	•charge: no
•spin: ½	•spin: 1
•magnetic moment: **- 1.91 μ_N**	•magnetic moment: no
•interaction with nuclei via scattering and absorption	•interaction via electrons in the atomic shell (Photo-, Compton-Effekt)

Neutron interactions

Neutron interaction with matter

Attenuation in specimen:





Attenuation (μ) of the neutron beam depends on:

- absorption (σ_{abs})
- scattering (σ_s)

$$\mu^{tot} = N_V\left(\sigma_{abs} + \sigma_s\right) = N_V\sigma^{tot}$$

N_V : number of atoms per unit volume

Mass attenuation coefficient (m^2/kg):

$\mu_m = \mu/\rho$,

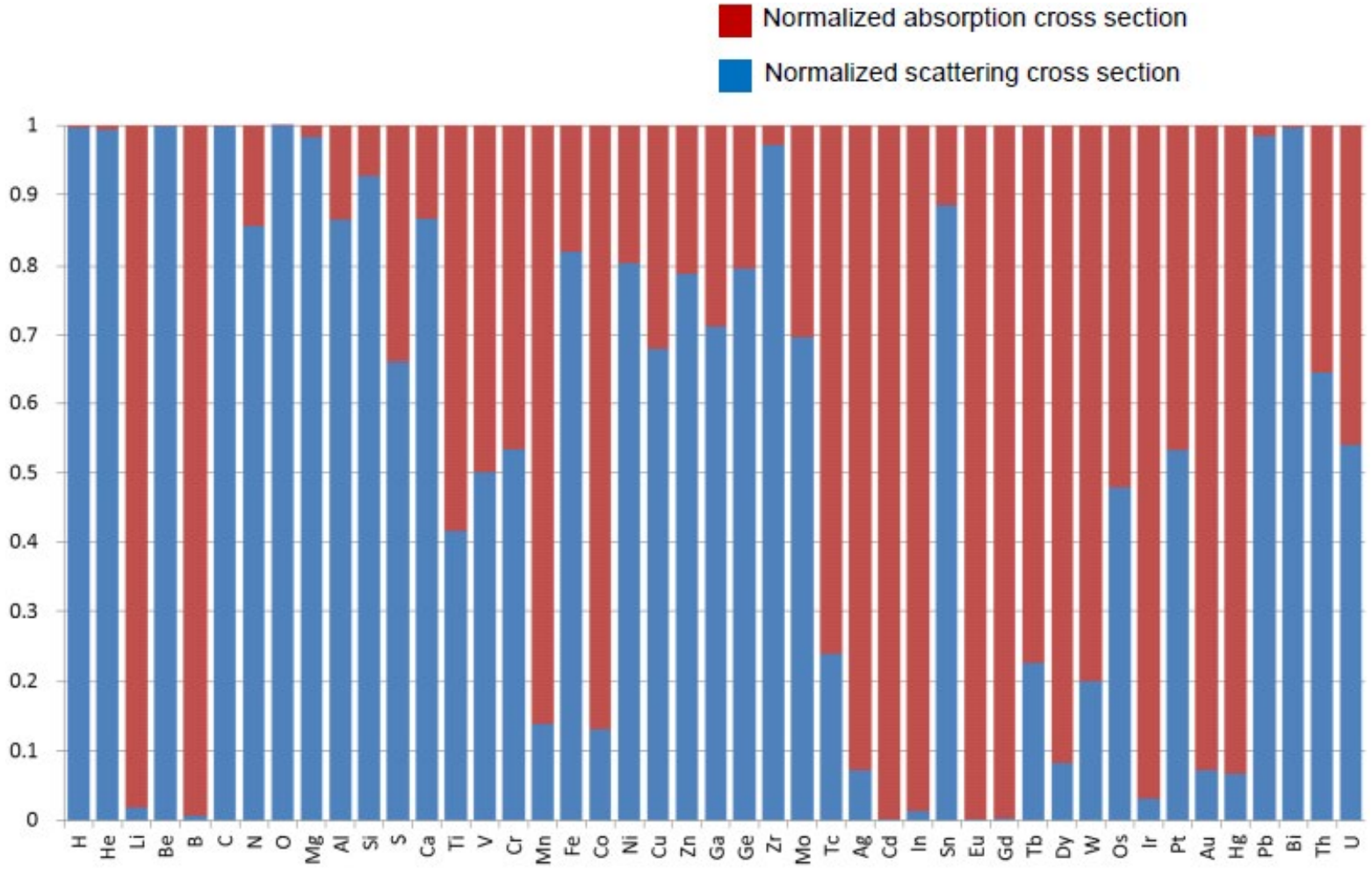
Lambert-Beer law:

$$I_D = I_0 exp\left(-\int_0^L \mu(t)dt\right)$$

$$I = I_o\, e^{-\mu(E)t} = I_o\, e^{-\frac{\mu(E)}{\rho}\rho t}$$

t- sample thickness, μ - attenuation coefficient

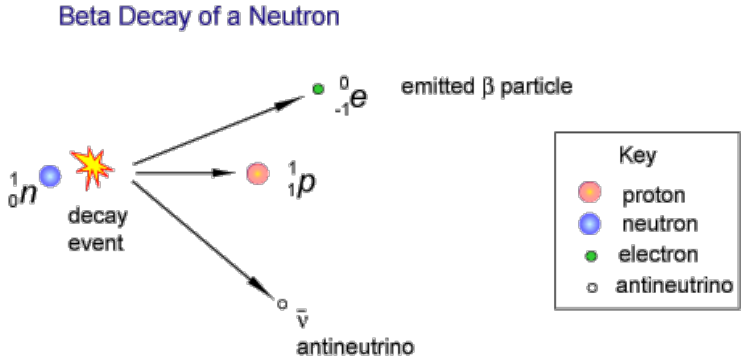
What reaction is thermal neutron imaging based on?



Neutron sources

Neutron production

Free neutrons are unstable (undergo beta- decay), they exist on long time scales only in bound state in the atomic nucleus.



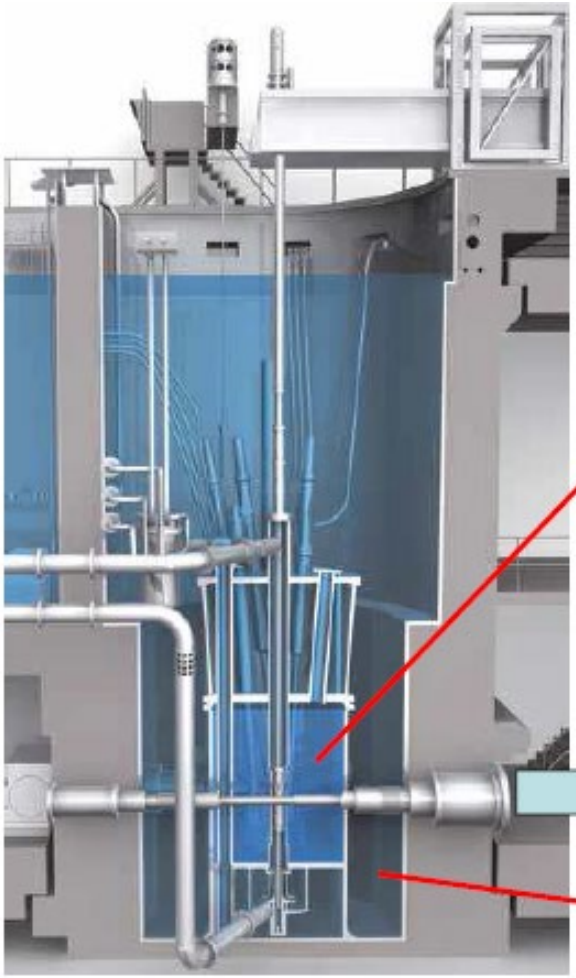
To create free neutrons they have to be continuously "freed" from the nucleus. A nuclear reaction is needed to break the nuclear binding forces in suitable nuclei.

Options:

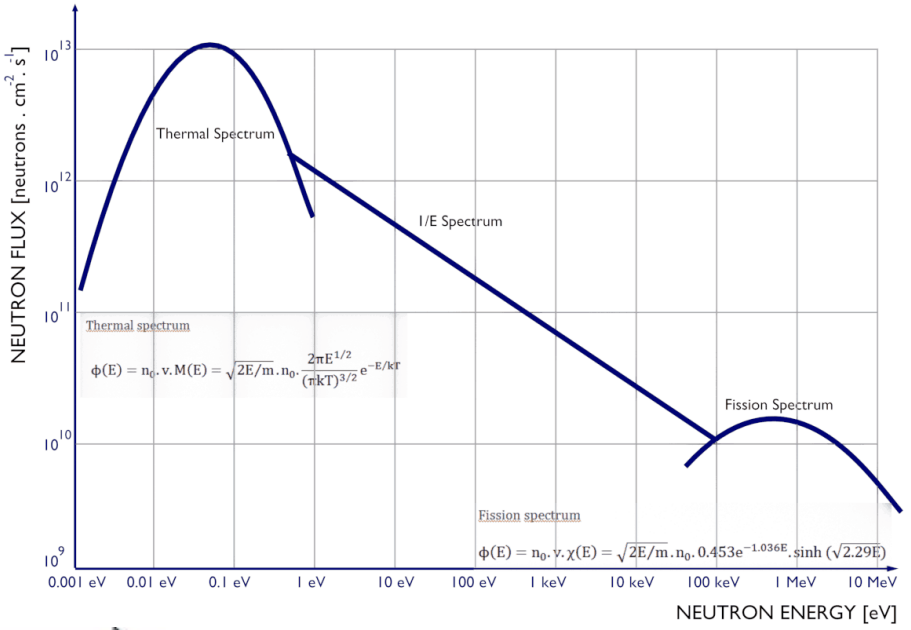
- various nuclear reactions by bombarding the nucleus
  high-E protons on heavy metal targets: spallation
  high-E protons, deuterons etc. on light target nuclei
  (α,n) reaction,
  (γ,n) reaction, photo neutrons } Isotopic sources

- fission: splitting of nuclei by neutrons
- utilizing spontaneous reactions: spontaneous fission

Neutron sources: reactors



Moderator tank (D_2O)

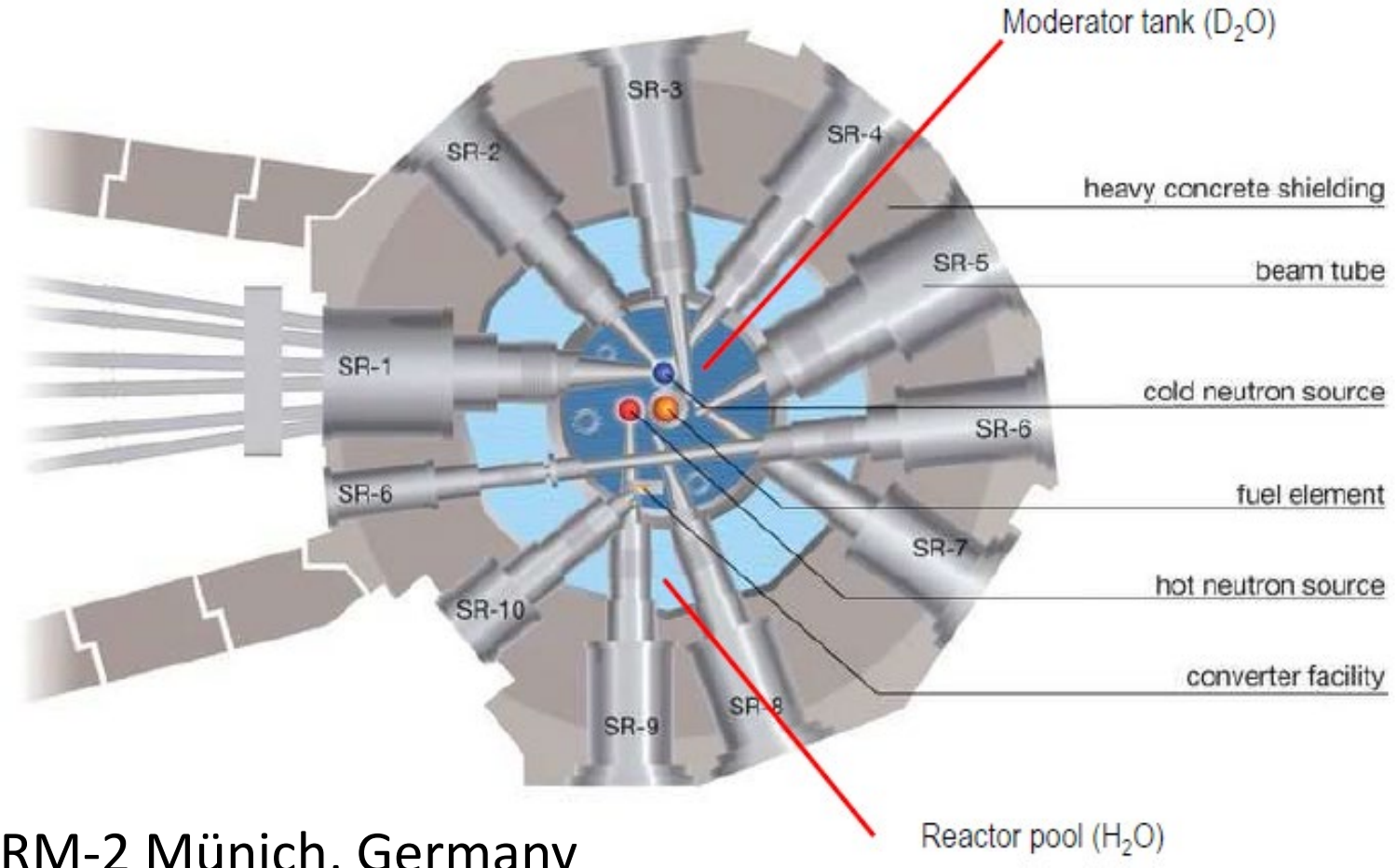


Beamline

Reactor pool (H_2O)

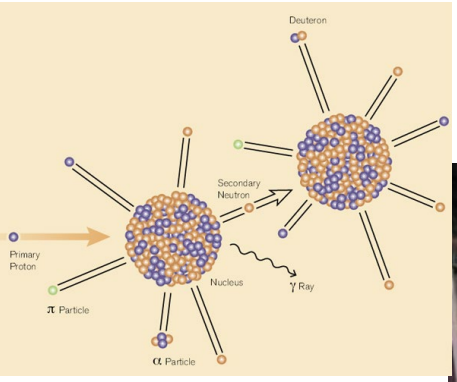
FRM-2 Münich, Germany

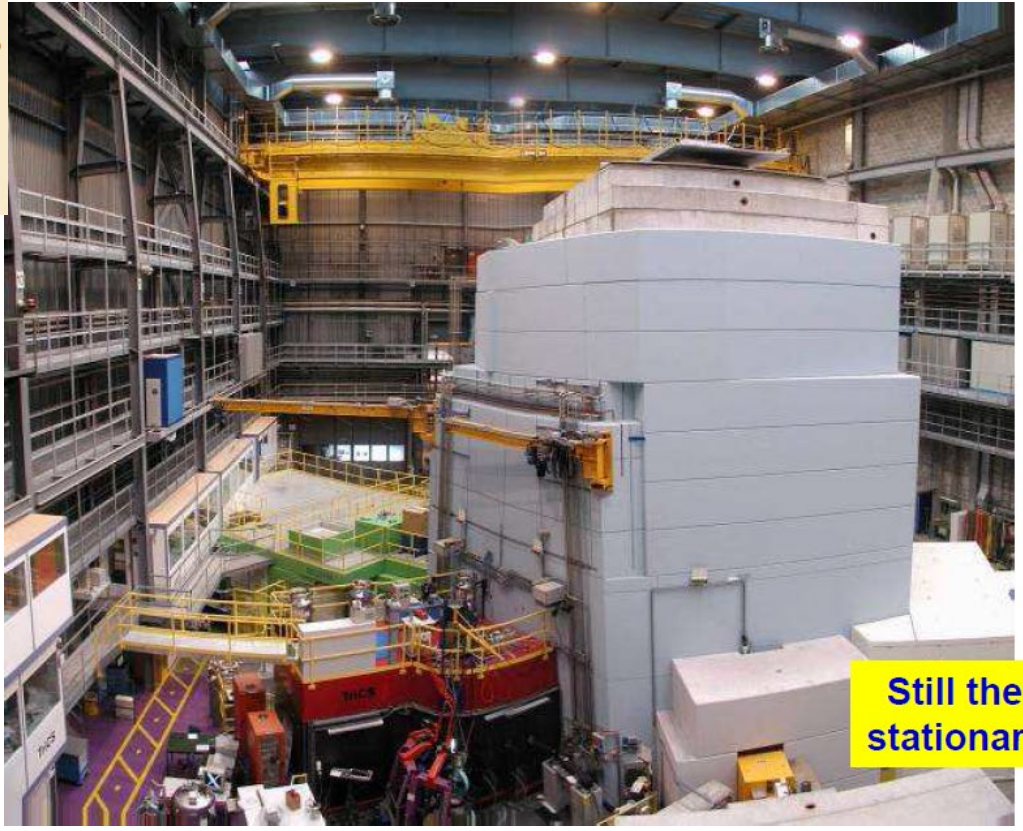
Neutron sources: reactors



FRM-2 Münich, Germany

Neutron sources: spallation



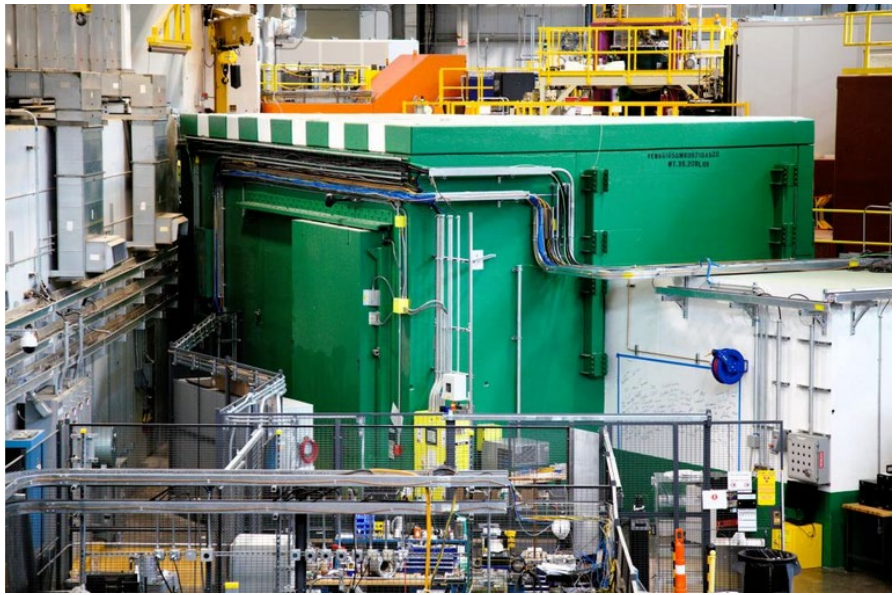


- In operation since 1997
- Driven by 590 MeV protons on a Pb target
- Intensity about 1.2 mA, corresponding to 1MW thermal power
- Installations for research with thermal and cold neutrons

Still the world's strongest stationary spallation source

Neutron sources: spallation

SNS: Oak Ridge National Laboratory

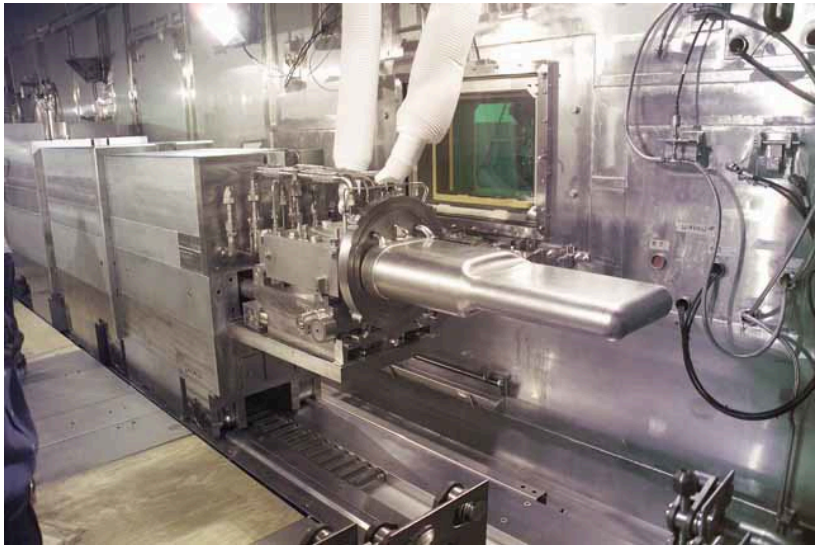


The VENUS imaging beam line started user operation spring 2026 at SNS!

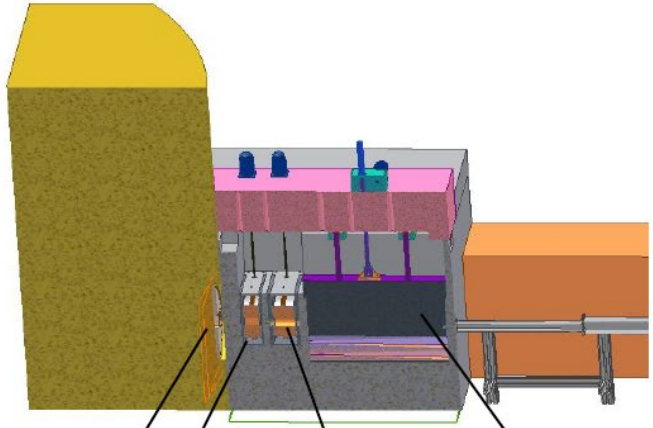
Short pulse spallation neutron sources!

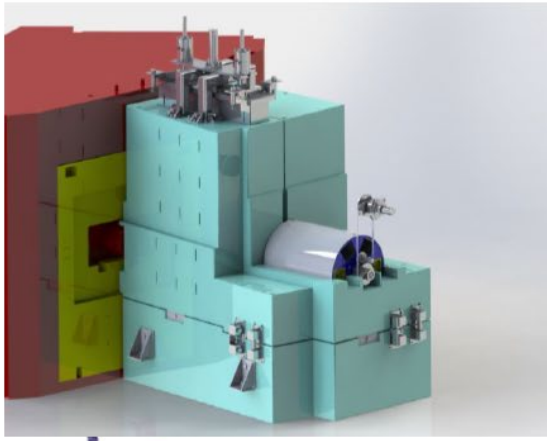
- Ion source (2.5 MeV)
- LINAC (2.5-1000 MeV)
- Proton accumulator ring (bunching for pulses)

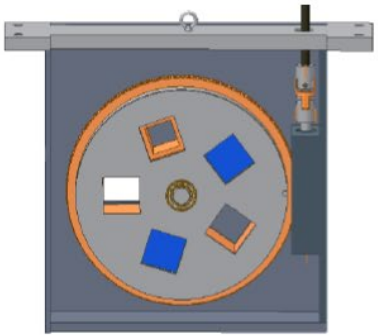
Target: liquid mercury. Cold moderator: liquid hydrogen at a temperature of 20 K



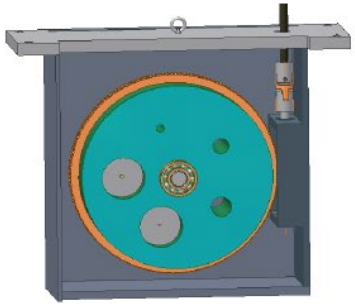
Neutron beam shaping (reactor & spallation)



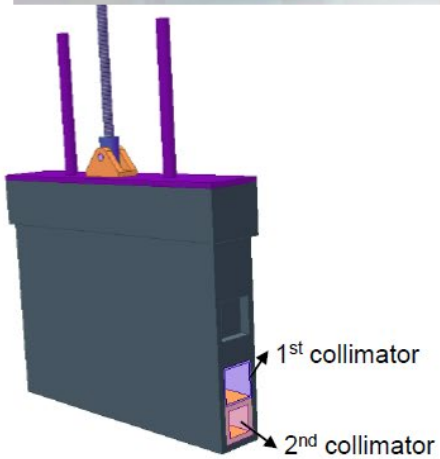




Filters



Pinhole collimators



Outer-collimator

Neutron beam shaping (reactor & spallation)

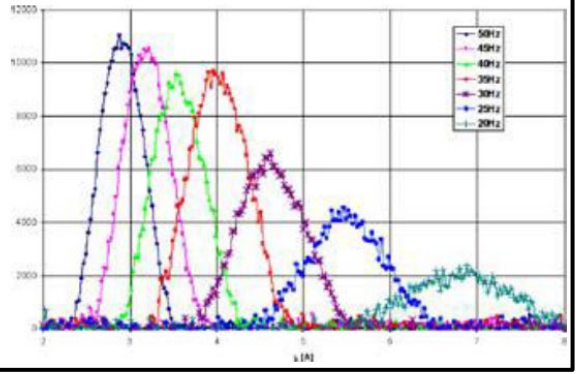


Neutron Velocity Selector

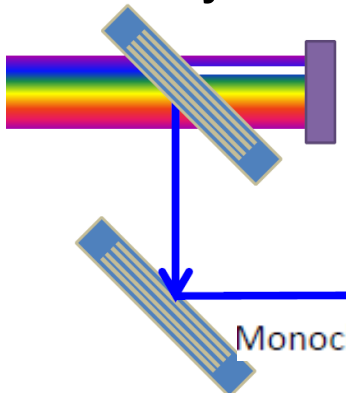
a device that allows neutrons of defined velocity to pass while absorbing all other neutrons, used for the purpose of producing a monochromatic neutron beam. The blades are coated with a strongly neutron-absorbing material







Double crystal monochromator:



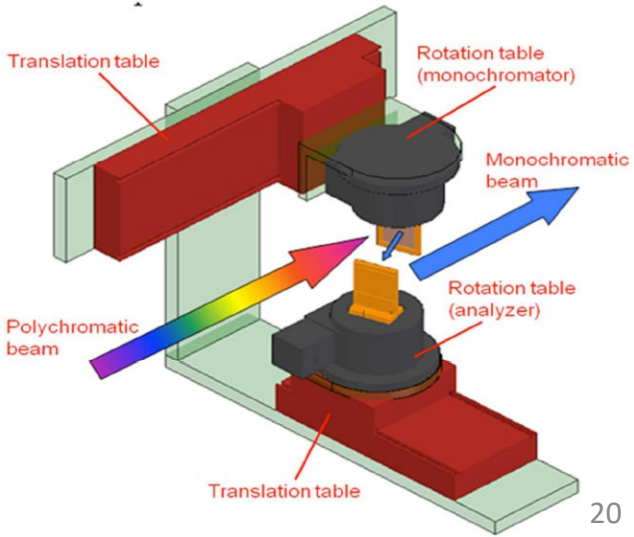
Bragg Law

$$2d \sin\theta = n\lambda$$

Set crystal angle to $\theta_1 \rightarrow \lambda_1$

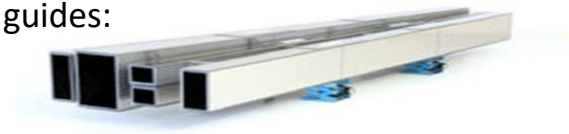
Second crystal parallel to bring it back in the original direction

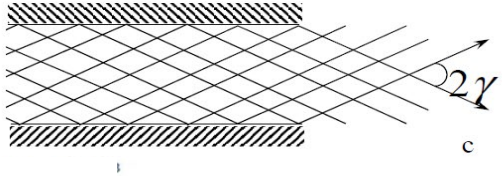
Monochromaticity $\Delta\lambda/\lambda$ ~1-3%

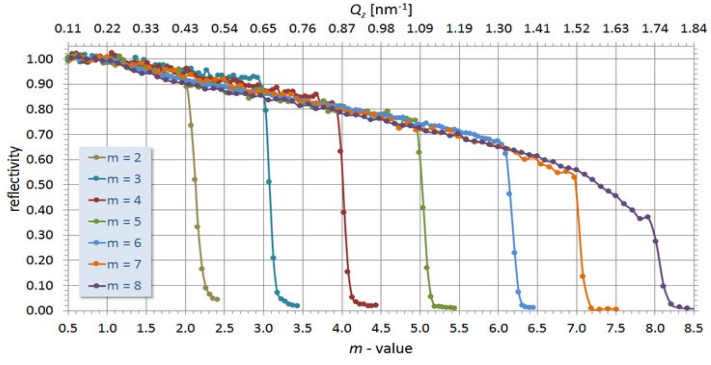


Neutron beam shaping (reactor & spallation)

Neutron guides:

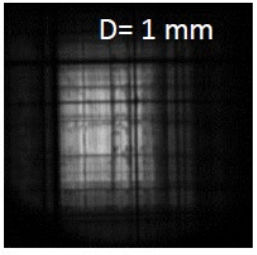


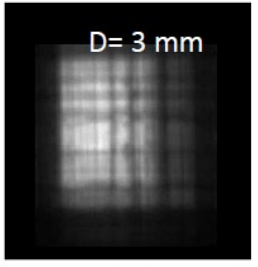


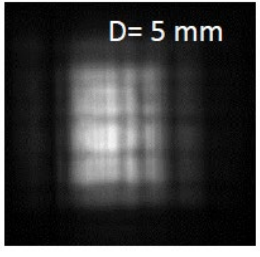


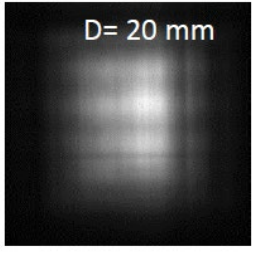
Lower limit L/D

$$L/D = 1/\tan(2\gamma_c(\lambda)).$$

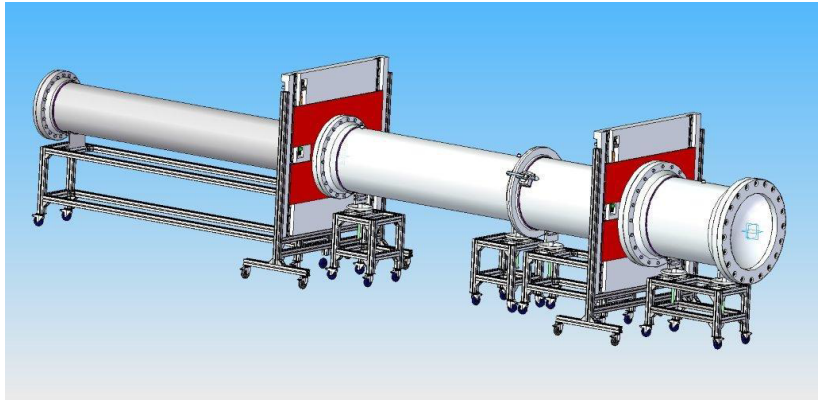


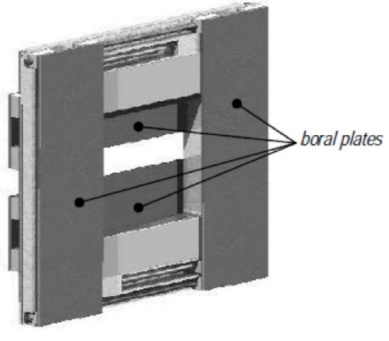






Neutron flight tubes & beam limiters:





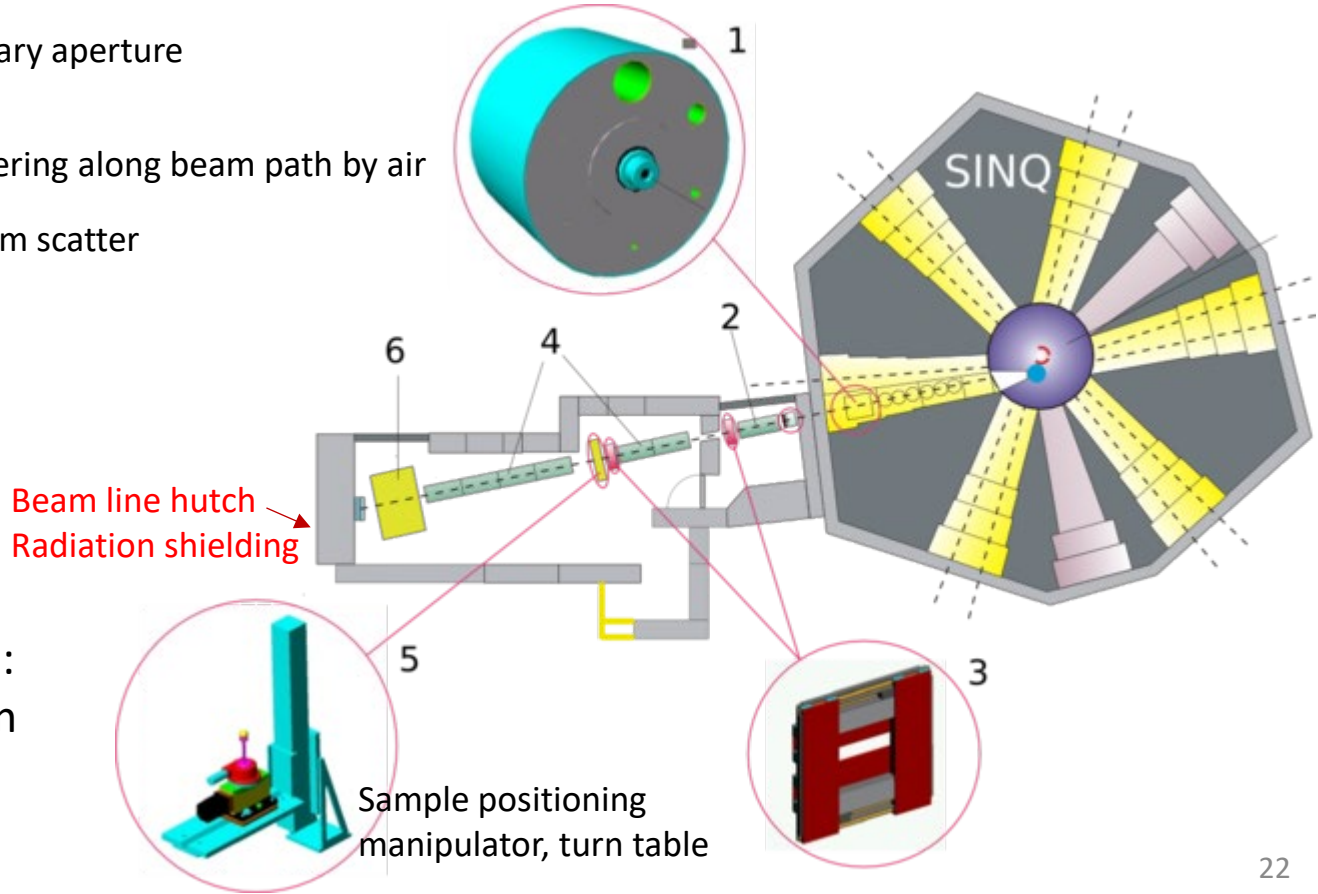
Neutron beam shaping, filtering

Pos	Main feature
1	Aperture wheel
2	Flight tube
3	Beam limiters
4	Flight tubes
5	Imaging of small to medium sized samples
6	Imaging of large samples

To select primary aperture

To minimize scattering along beam path by air

To minimize room scatter



ICON cold beam line, SINQ, PSI:
Direct line of sight on spallation source -> gamma contribution

Neutron imaging detectors

Neutron detectors: reactions

Q values

$^{3}He + {}^{1}n \rightarrow {}^{3}H + 1p + 0.764\ MeV, \sigma=5333b$

$^{6}Li + {}^{1}n \rightarrow {}^{3}H + {}^{4}He + 4.79\ MeV, \sigma=940b$

XS values are given at 25meV

$^{10}B + {}^{1}n \rightarrow {}^{7}Li + {}^{4}He + 2.79\ MeV, \quad (7\%)$

$\rightarrow {}^{7}Li^{*} + {}^{4}He + 2.31\ MeV + \gamma\ (0.48\ MeV) \quad (93\%)$

$\sigma=3835b$

$^{155}Gd + {}^{1}n \rightarrow {}^{156}Gd + \gamma\ (7.9\ MeV) + \text{conversion electrons}, \sigma=49700b$

$^{157}Gd + {}^{1}n \rightarrow {}^{158}Gd + \gamma\ (8.5\ MeV) + \text{conversion electrons}, \sigma=255000b$

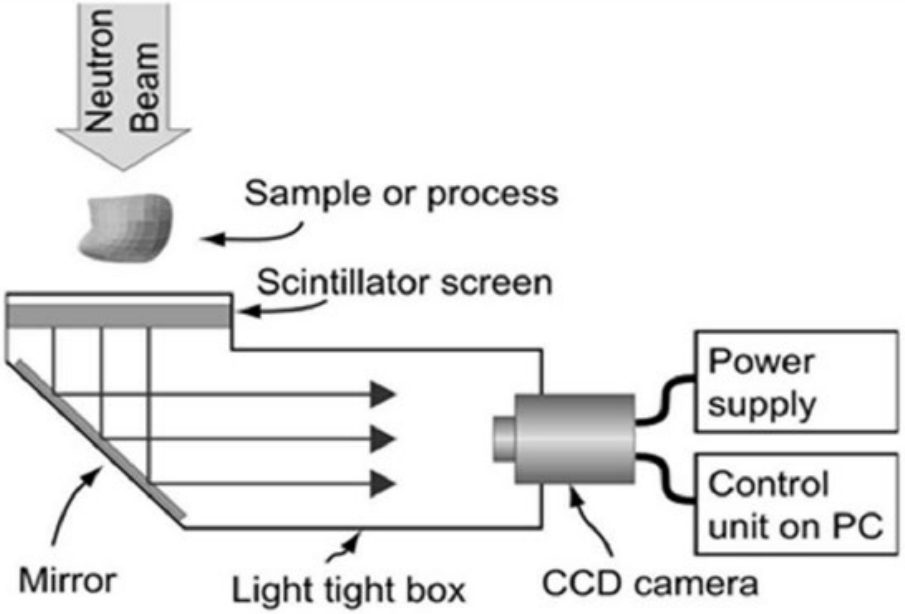
$^{235}U + {}^{1}n \rightarrow \text{fission products} + \sim 200\ MeV, \sigma=681b$

Only the ^{3}He and the ^{6}Li reactions are not accompanied by the release of γ radiation -> background!

Neutron imaging detectors

Main components:

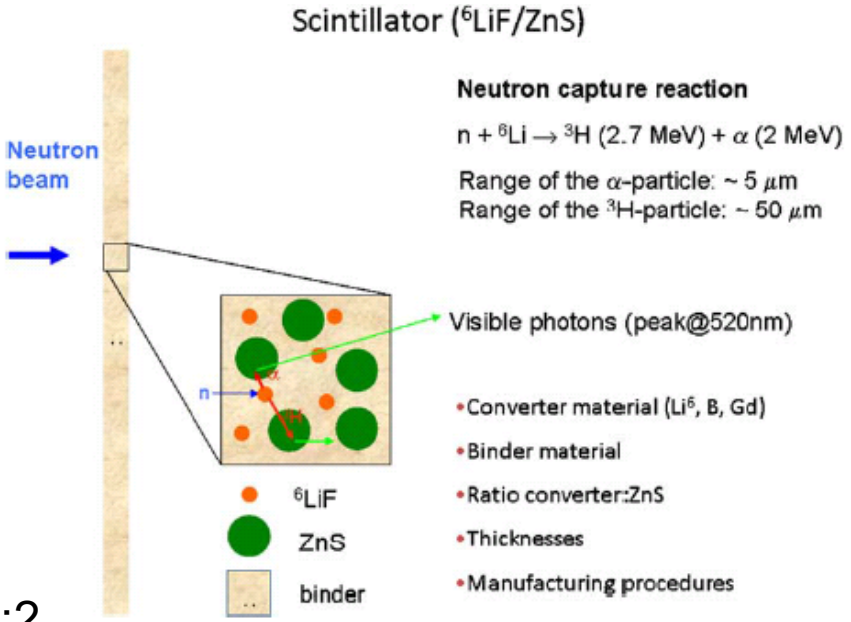
- Scintillator/converter screen
- Mirror to steer light into the camera. It enables removing camera from direct beam or a better shielding of it (radiation damage).
- CCD/CMOS camera
- Optional: Image intensifier between scintillator and camera
- Light tight box



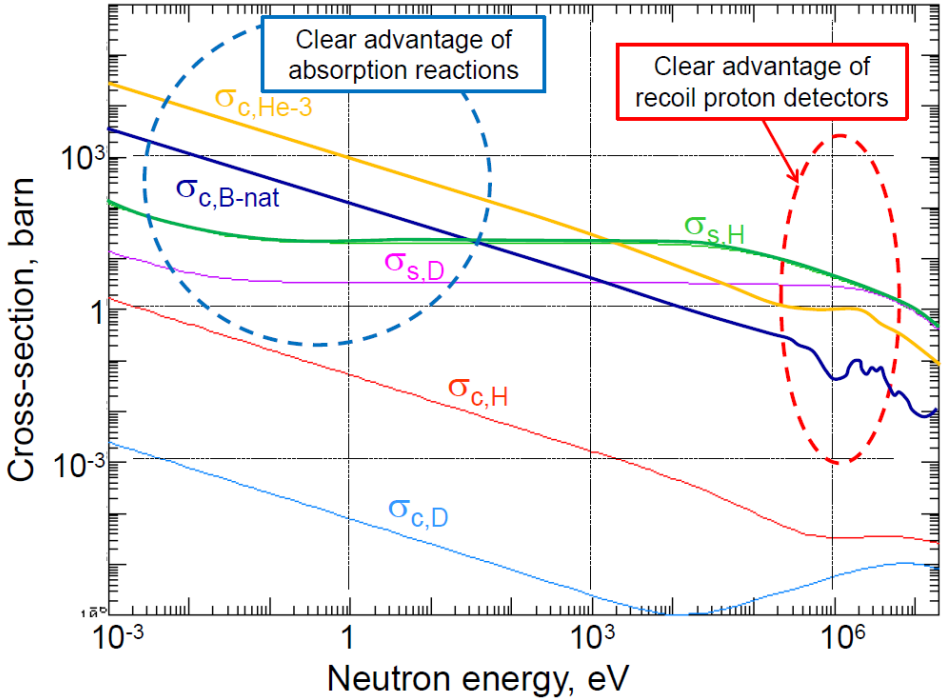
Li-based scintillator screens

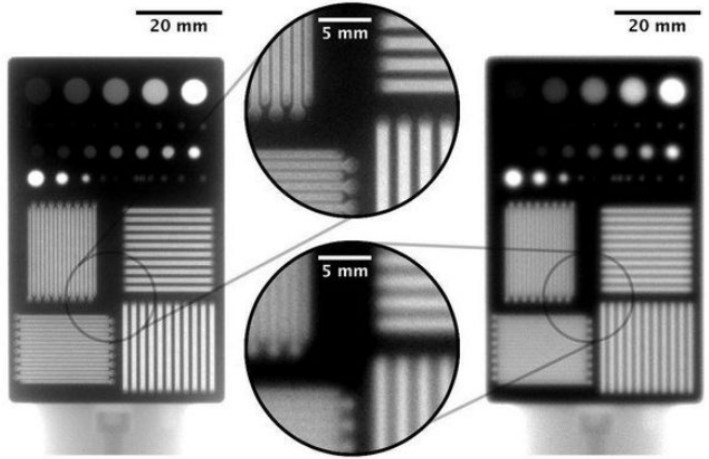
LiF/ZnS:Ag or LiF/ZnS:Cu scintillators:

- Two (three) components scintillator:
  - neutron absorber (^{6}LiF)
  - phosphor/light emitter (ZnS)
  - (in)organic binder
- Very high Q value
- very high light output: 160'000 ph/n
- light output optimized ratio of LiF and ZnS is 1:2
- typical scintillator layer thicknesses available 50-450 μm (for the latter self-shielding starts to play a role)
- the smaller thickness the higher resolution <-> the higher thickness the higher detection efficiency



Fast neutron scintillators





Radiography of an iron block measured with the 2 different scintillator types. Left with the 2 layer PE (3 mm) / ZnS:Ag (60 µm) and right with the standard 2.4 mm PP / ZnS:Cu (30%) scintillator

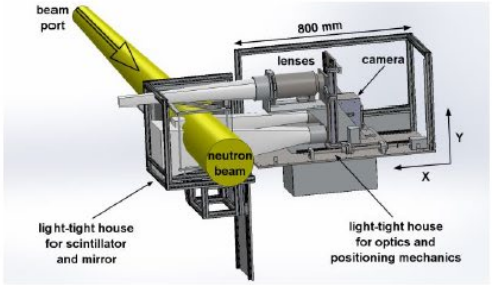
Source: RcTritec, https://www.rctritec.com/en/isotopes/scintillators-for-fast-neutrons-1

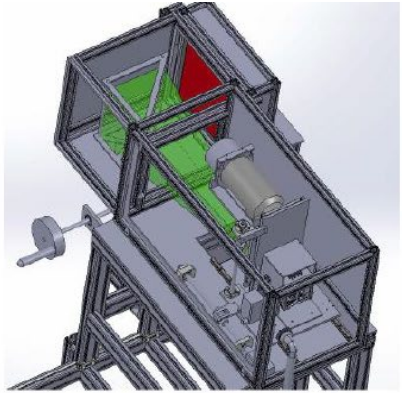
In the ≥ 1 MeV energy range the neutron interaction XS are generally 2-3 order of magnitude lower for each material than for thermal/cold neutrons.

Elastic scatter process on light elements to convert fast neutrons becomes the most interesting detection option! Scatter on hydrogen produces recoil protons.

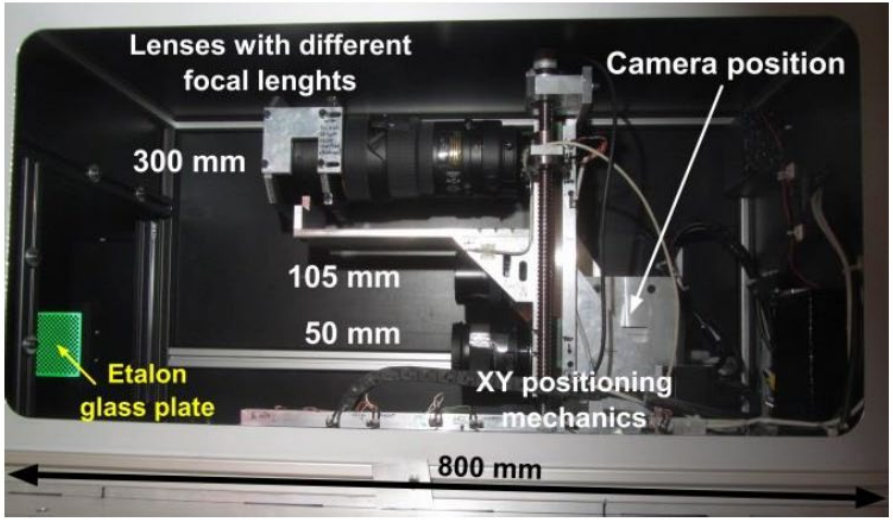
Hydrogen-rich plastic (organic) scintillators are commonly used for fast neutron detection!

Digital imaging detector of RAD beam line



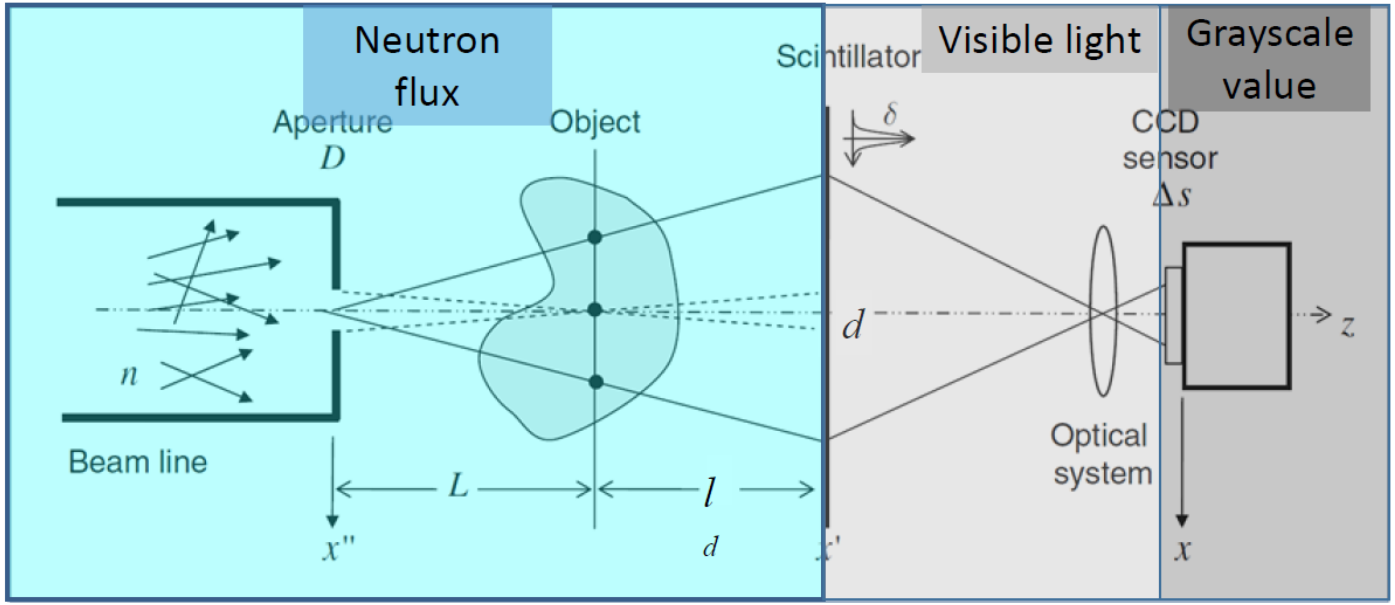


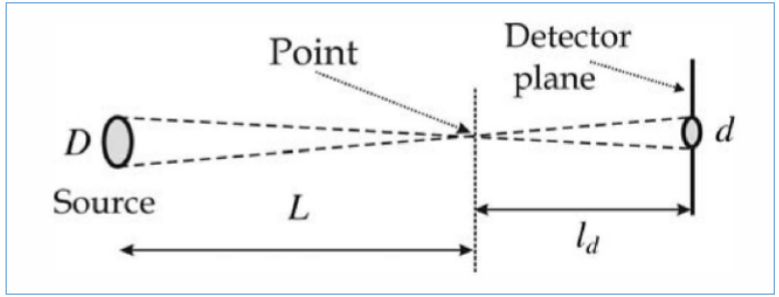






Beam collimation, L/D, spatial resolution





A larger L/D ratio provides better image resolution because image blur (*d*) is smaller.

$$\frac{L}{D} = \frac{l_d}{d}$$

How close the beam geometry is to the ideal point-source configuration?

Geometrical unsharpness (blur, penumbra), d:

$$\mathrm{d} = \frac{l_d}{\mathrm{L/D}}$$

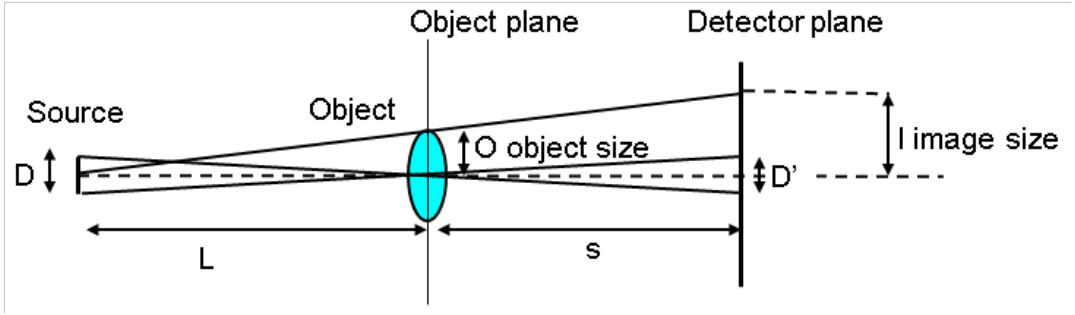
Overall resolution of imaging setup

Object magnification: $\boldsymbol{M} = \frac{I}{O} = \frac{L+s}{L} = 1 + M_s$

Source magnification: $M_s = \frac{D'}{D} = \frac{s}{L} = \mathrm{M} - 1 \rightarrow$

$D' = \frac{s}{L/D} = (M-1)D$

The geometric blur by the finite source size projected through the object plane



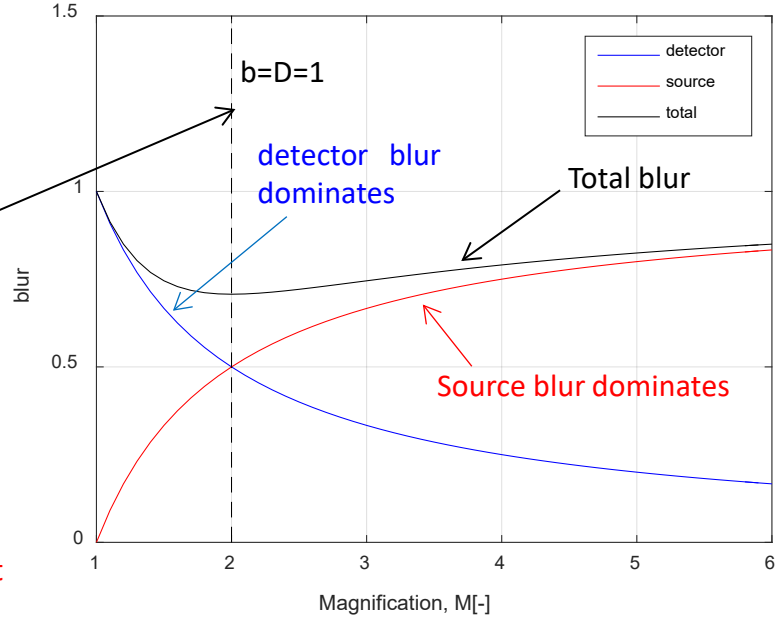
The source blur in the object plane: $B_s = (M-1)D/M$

Blur by the detector *b*, in the object plane: $B_d = \mathrm{b/M}$

Total blur (root-mean square of component's blur):

$$B = \sqrt{{B_s}^2 + {B_d}^2} = \sqrt{\frac{(M-1)^2 D^2}{M^2} + \frac{b^2}{M^2}}$$

Minimum occurs when $b^2 = (\mathrm{M}-1)D^2 \rightarrow M = 1 + \frac{b^2}{D^2}$



For micro-focus X-ray setup at high magnification (M>>1):

$$B = \sqrt{{B_s}^2 + {B_d}^2} \cong \sqrt{{B_s}^2} \cong D$$

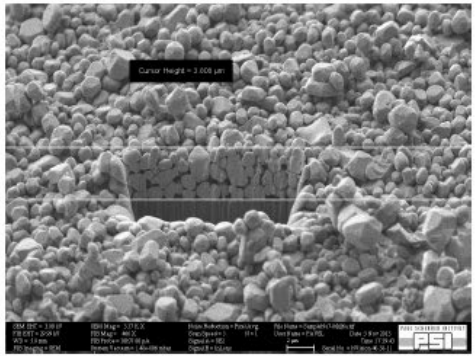
Small D is needed for high resolution

Micro-focus X-ray CT pixel/voxel size for high M:

$$pix_{CT} = pix_{detector}/\mathrm{M}$$

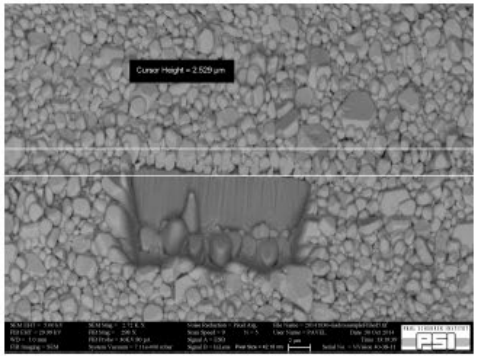
Detector pixel size is not limiting too much

High resolution detection by thin Gadox scintillator



4µm

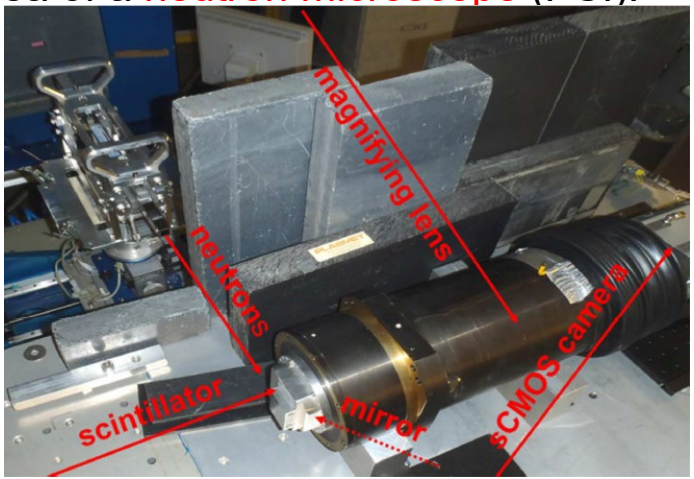
Trtik et al., Physics Proc., (2015)

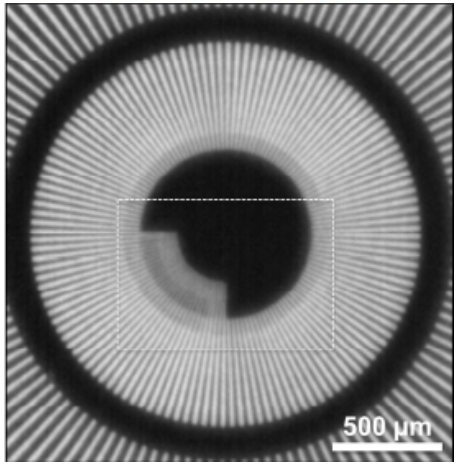


2.5µm

Trtik & Lehmann, ECNS, 2015

Idea of a neutron microscope (PSI):





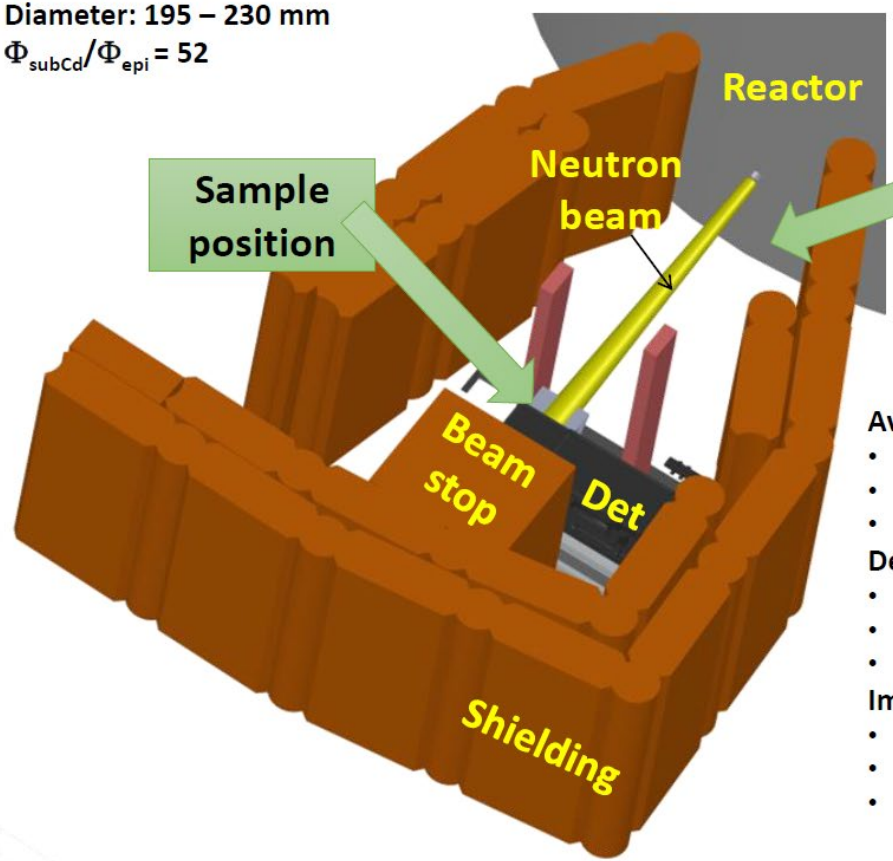
Trtik et al., Phys. Proc. (2015)

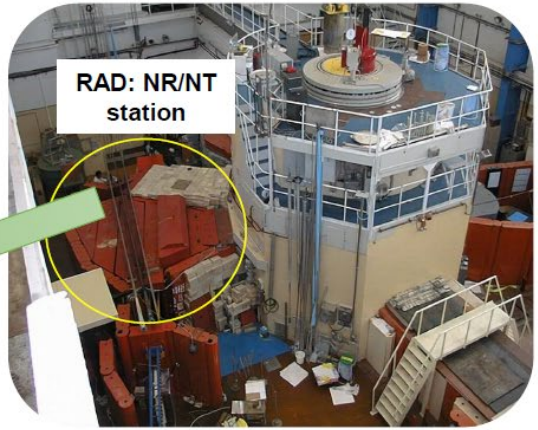
Pixel size: 1.65 µm, Resolution: 7.6 µm

Long exposure times are needed for reasonable image statistics!

RAD beam line @ BNC

Primary aperture to screen distance: 463 – 539 cm
Flux: 4.6 – 3.38 × 10^7 cm^{-2} s^{-1}
L/D = 170 – 195
Diameter: 195 – 230 mm
Φ_{subCd}/Φ_{epi} = 52





Available modalities:
- Thermal neutron
- Gamma beam: ~ 8.5 Gy/h
- X-ray tube: 25-225 keV, max. 10 mA

Detector options:
- 16-bit 4 Mpx sCMOS camera
- Highly sensitivity TV-camera
- Image plate

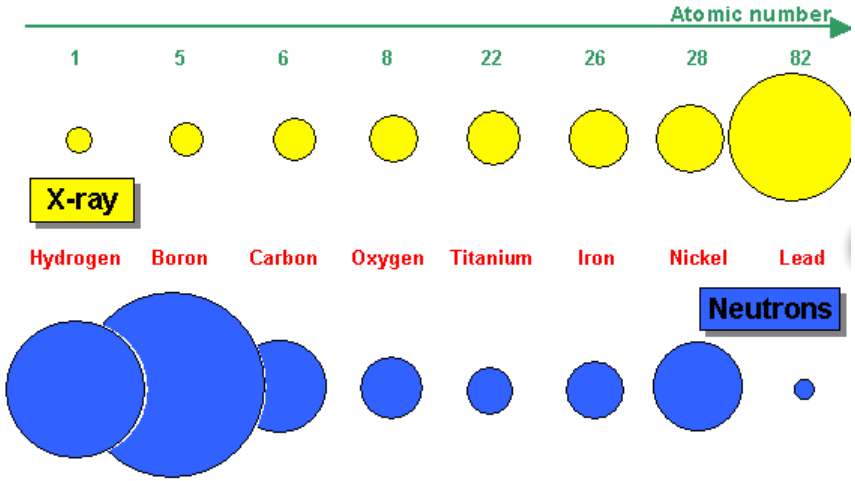
Imaging options:
- Radiography or Tomography of larger objects
- Small FOV, better resolution
- (Sapphire filter to get rid of fast neutrons)

Neutrons vs. X-rays

X-ray vs. thermal neutron imaging

X-ray: interaction with electron shell: photo-electric effect, Compton scatter

high-Z sensitivity



light element sensitivity, high-Z transparence

Neutron vs. X-ray: interaction with the nucleus vs. electron shell

Attenuation coefficients for thermal neutrons [cm^{-1}]

1a	2a	3b	4b	5b	6b	7b	8			1b	2b	3a	4a	5a	6a	7a	0
H																	He
3.44																	0.02
Li	Be											B	C	N	O	F	Ne
3.30	0.79											101.60	0.56	0.43	0.17	0.20	0.10
Na	Mg											Al	Si	P	S	Cl	Ar
0.09	0.15											0.10	0.11	0.12	0.06	1.33	0.03
K	Ca	Sc	Ti	V	Cr	Mn	Fe	Co	Ni	Cu	Zn	Ga	Ge	As	Se	Br	Kr
0.06	0.08	2.00	0.60	0.72	0.54	1.21	1.19	3.92	2.05	1.07	0.35	0.49	0.47	0.67	0.73	0.24	0.61
Rb	Sr	Y	Zr	Nb	Mo	Tc	Ru	Rh	Pd	Ag	Cd	In	Sn	Sb	Te	I	Xe
0.08	0.14	0.27	0.29	0.40	0.52	1.76	0.58	10.88	0.78	4.04	115.11	7.58	0.21	0.30	0.25	0.23	0.43
Cs	Ba	La	Hf	Ta	W	Re	Os	Ir	Pt	Au	Hg	Tl	Pb	Bi	Po	At	Rn
0.29	0.07	0.52	4.99	1.49	1.47	6.85	2.24	30.46	1.46	6.23	16.21	0.47	0.38	0.27			
Fr	Ra	Ac	Rf	Ha													
	0.34																

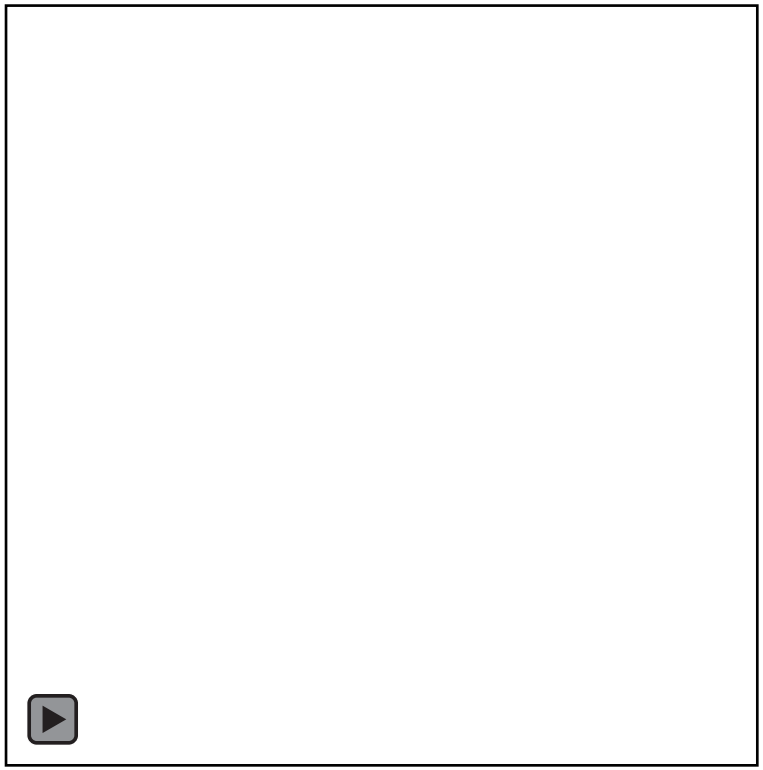
	Ce	Pr	Nd	Pm	Sm	Eu	Gd	Tb	Dy	Ho	Er	Tm	Yb	Lu
*Lanthanides	0.14	0.41	1.87	5.72	171.47	94.58	1479.04	0.93	32.42	2.25	5.48	3.53	1.40	2.75
	Th	Pa	U	Np	Pu	Am	Cm	Bk	Cf	Es	Fm	Md	No	Lr
**Actinides	0.59	8.46	0.82	9.80	50.20	2.86								

Attenuation coefficients for X-ray [cm^{-1}] (150kV)

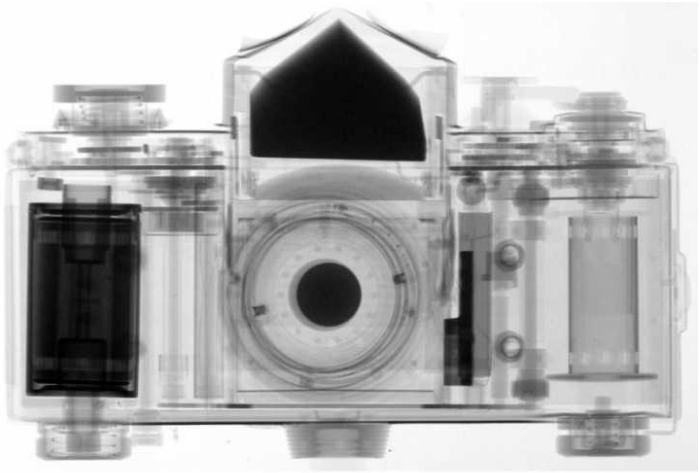
1a	2a	3b	4b	5b	6b	7b	8			1b	2b	3a	4a	5a	6a	7a	0
H																	He
0.02																	0.02
Li	Be											B	C	N	O	F	Ne
0.06	0.22											0.28	0.27	0.11	0.16	0.14	0.17
Na	Mg											Al	Si	P	S	Cl	Ar
0.13	0.24											0.38	0.33	0.25	0.30	0.23	0.20
K	Ca	Sc	Ti	V	Cr	Mn	Fe	Co	Ni	Cu	Zn	Ga	Ge	As	Se	Br	Kr
0.14	0.26	0.48	0.73	1.04	1.29	1.32	1.57	1.78	1.96	1.97	1.64	1.42	1.33	1.50	1.23	0.90	0.73
Rb	Sr	Y	Zr	Nb	Mo	Tc	Ru	Rh	Pd	Ag	Cd	In	Sn	Sb	Te	I	Xe
0.47	0.86	1.61	2.47	3.43	4.29	5.06	5.71	6.08	6.13	5.67	4.84	4.31	3.98	4.28	4.06	3.45	2.53
Cs	Ba	La	Hf	Ta	W	Re	Os	Ir	Pt	Au	Hg	Tl	Pb	Bi	Po	At	Rn
1.42	2.73	5.04	19.70	25.47	30.49	34.47	37.92	39.01	38.61	35.94	25.88	23.23	22.81	20.28	20.22		9.77
Fr	Ra	Ac	Rf	Ha													
	11.80	24.47															

	Ce	Pr	Nd	Pm	Sm	Eu	Gd	Tb	Dy	Ho	Er	Tm	Yb	Lu
*Lanthanides	5.79	6.23	6.46	7.33	7.68	5.66	8.69	9.46	10.17	10.91	11.70	12.49	9.32	14.07
	Th	Pa	U	Np	Pu	Am	Cm	Bk	Vf	Es	Fm	Md	No	Lr
**Actinides	28.95	39.65	49.08											

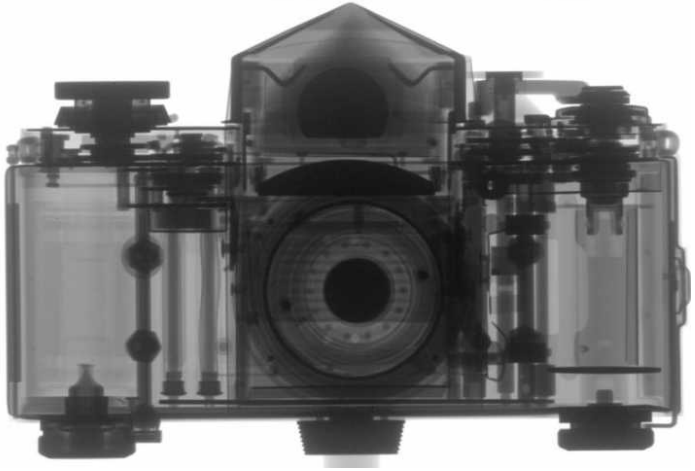
X-ray vs. thermal neutron imaging



source: https://www.youtube.com/watch?v=VESMU7JfVHU



Neutrons



X-rays

X-ray vs. neutron imaging, The figures

X-rays

Lab setups

- Intensity = large neutrons source
- Resolution - high, down to 500 nm
- Penetration - good for soft matter modest for metals/hard matter
- Time resolution - limited
- CT scan times - hours

Neutrons

- Intensity similar to lab X-ray sources
- Resolution – modest in general 50-100 um neutron microscope: 3-5 um
- Penetration - very good for metal and dense material but not for organic/plastic/water and some light elements
- Time resolution - limited
- CT scan times - hours

Synchrotrons

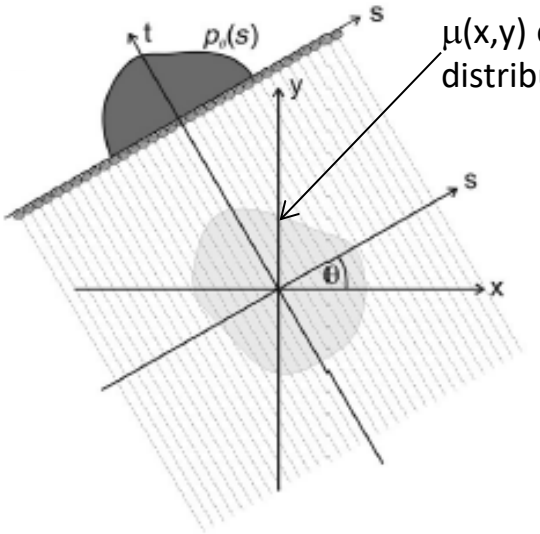
- excel in everything: 6 order of magnitude higher flux, very high resolution, fast imaging
- Mostly low energy - soft matters



Intensity matters!

Computed Tomography principles

Radon transform



μ(x,y) object distribution

Coordinate transform (x,y) ->(s,t):

$$\begin{pmatrix} s \\ t \end{pmatrix} = \begin{pmatrix} cos\theta & sin\theta \\ -sin\theta & cos\theta \end{pmatrix} \begin{pmatrix} x \\ y \end{pmatrix}$$

Equation of a line for *s=const.* and *t=arb.*:

$$s = xcos\theta + ysin\theta$$

Using the Dirac distribution to express a **line integral** in 2D:

$$\int_{-\infty}^{+\infty} \delta(z)dz = 1 \qquad z = s - xcos\theta - ysin\theta$$

The line integral of the 2D distribution μ(x,y):

$$p(s,\theta) = \iint_{-\infty}^{+\infty} \delta(s - xcos\theta - ysin\theta)\mu(x,y)dxdy$$

Johann Radon (1917)



This is the **Radon transformation** of μ(x,y) from real space (x,y) into the (s,θ) Radon space of line parameters:

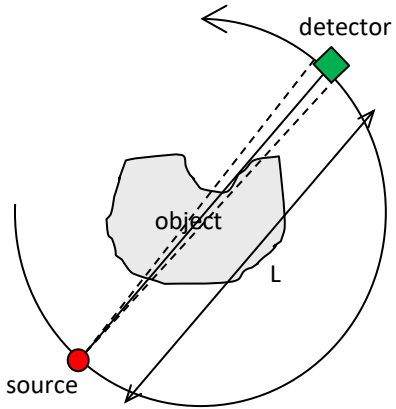
$$p(s,\theta) = \Re\{\mu(x,y)\}$$

p is the projection of the μ(x,y) object

This transformation is the so-called forward projection!

Radon transform & filtered backprojection

Connection between the Radon transform and the Lambert-Beer law for transmission tomography:



$$I_D = I_0 exp\left(-\int_0^L \mu(t)dt\right)$$

$$E = -ln\frac{I_D}{I_0} = \int_0^L \mu(t)dt$$

I_D – intensity measured by detector element/pixel behind the sample

I_0 – intensity measured by detector element/pixel without sample

$$p(s,\theta) = -ln\frac{I_D}{I_0} = \iint \delta(s - xcos\theta - ysin\theta)\mu(x,y)dxdy$$

The **analytical inverse** in 2D (Radon, 1917):

$$\mu(x,y) = \frac{1}{2\pi^2}\int_0^{\pi}\int_{-\infty}^{+\infty}\frac{1}{xcos\theta + ysin\theta - s}\frac{\partial p(s,\theta)}{\partial s}dsd\theta$$

In the Fourier domain:

Filtered backprojection

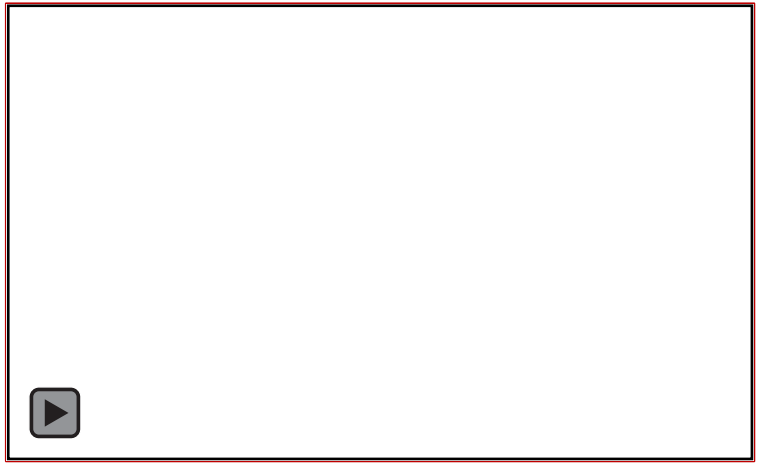
$$\mu(x,y) = \frac{1}{2\pi}\int_0^{\pi}\left[\int_{-\infty}^{\infty}\mathcal{F}\{p_\theta\}(r)e^{i2\pi rs}|r|dr\right]d\theta$$

CT principles

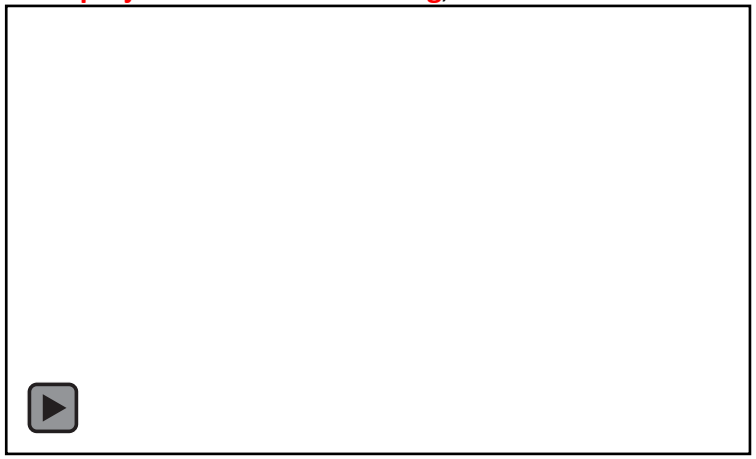
Forward projection, CT acquisition



Backprojection, CT reconstruction

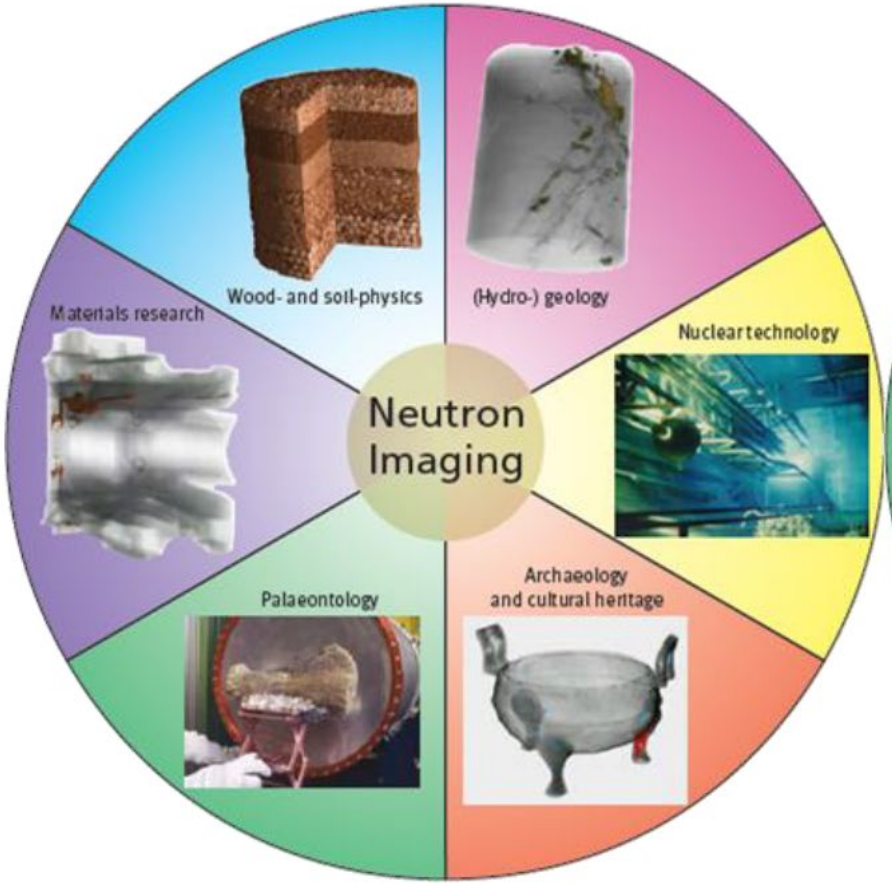


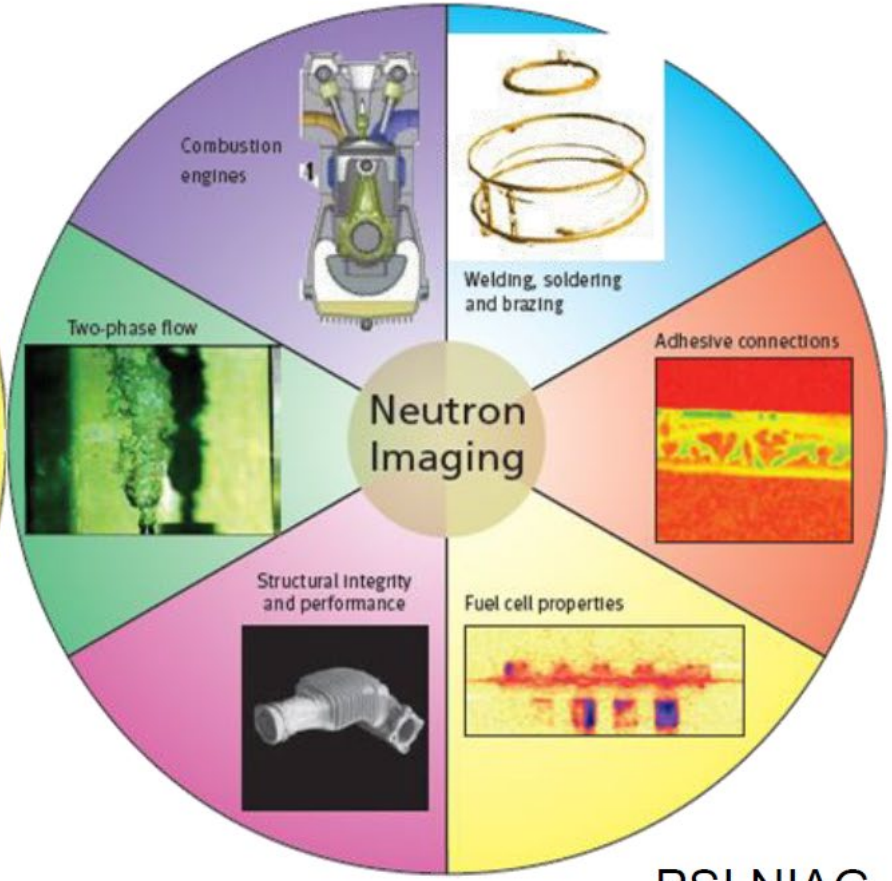
Backprojection without filtering, CT reconstruction



Applications of neutron imaging

Applications of neutron imaging: science+industry



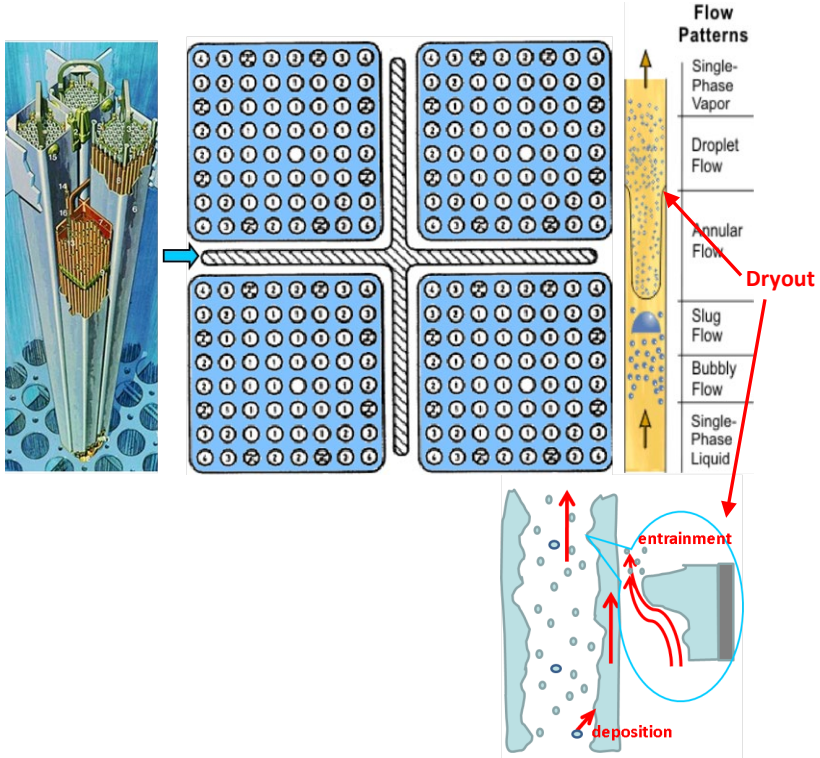


PSI NIAG

Applications in energy engineering

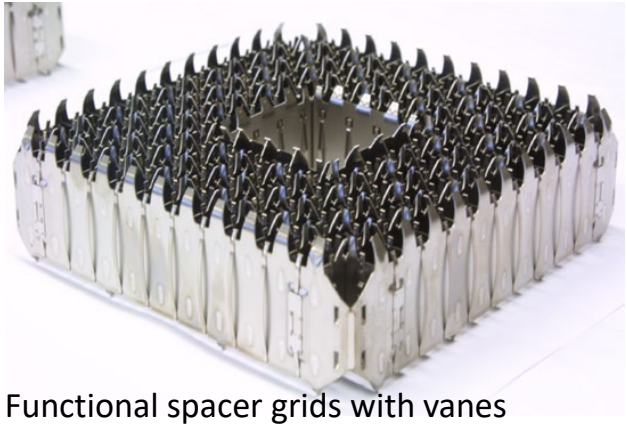
Nuclear Fuel Bundle research: Background and Motivation

MOTIVATION: Instrumentation development for nuclear fuel bundle studies and optimization: two-phase flows in fuel bundles!



Fuel bundle model studies to:

- optimize mixing and heat transfer in bundle
- safely increase margins to thermal (boiling) crisis, e.g. dry out
- safety and economy of fuel utilization

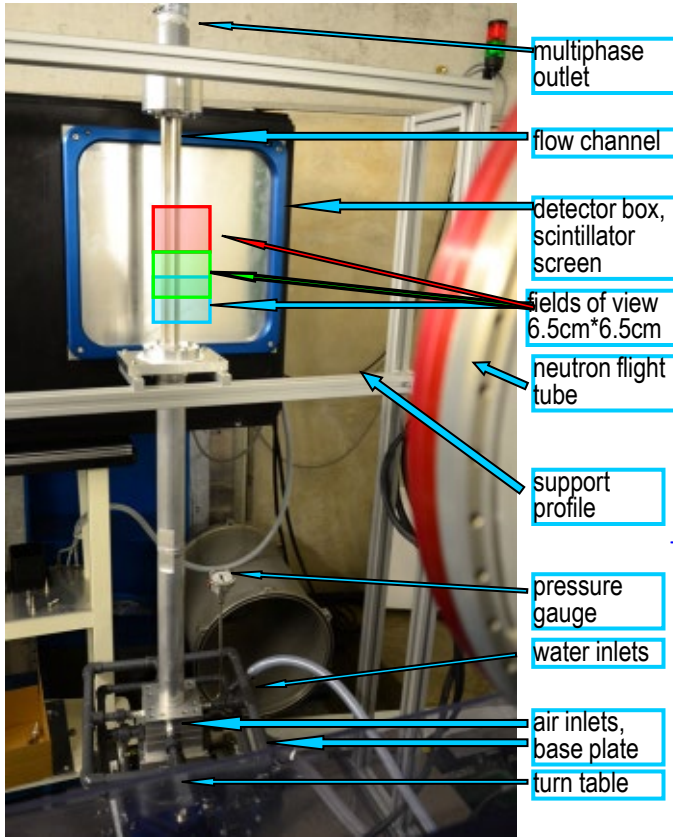


Functional spacer grids with vanes
Atrium 12 TM ,
AREVA

Need for high-resolution, non-intrusive, field measurement techniques and instrumentation! for both prototypical experiments (vendors), or non-prototypical conditions (code validation)

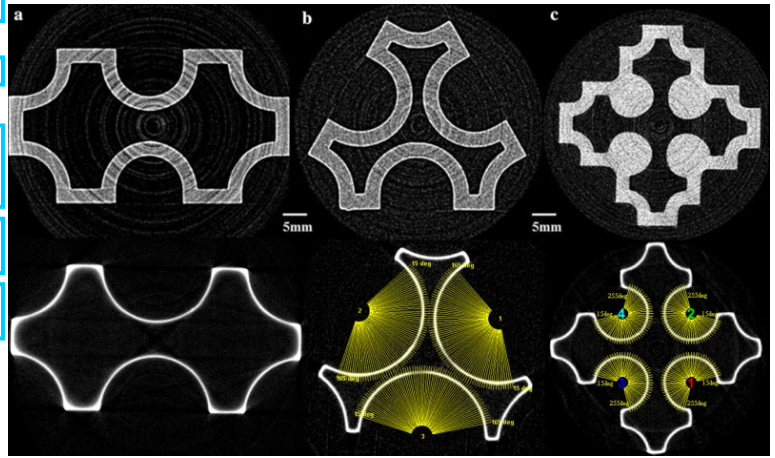
Cold Neutron Imaging of Adiabatic Flows 1.

Subchannel mockup at the beam line:

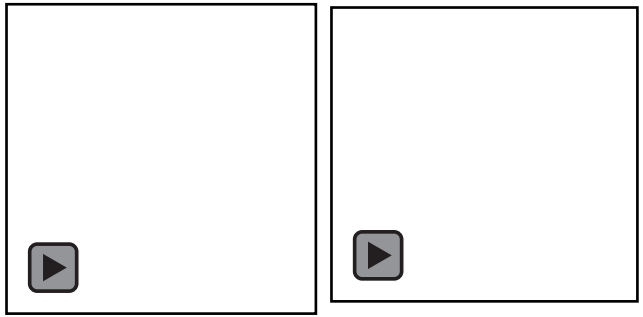


Adiabatic, air-water annular flows

Tomographic reconstruction of the empty channel cross section



Tomographic reconstruction of the water film inside the subchannels

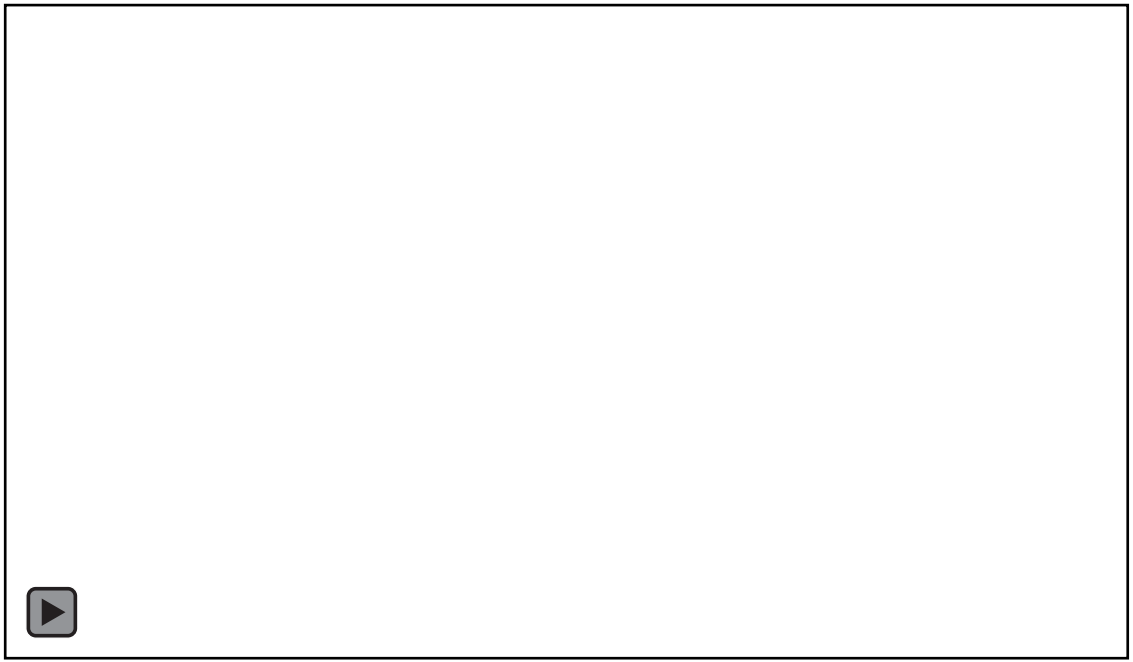


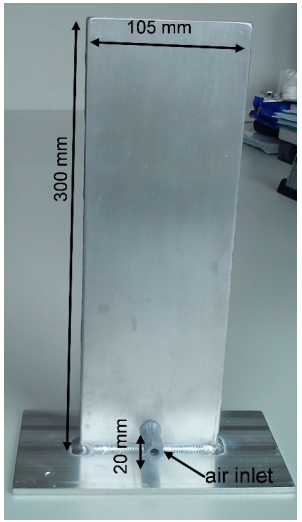
Time-averegd results, neutron CT takes several hours!

High speed NI of two-phase flows in a bubbler

Imaging setup:

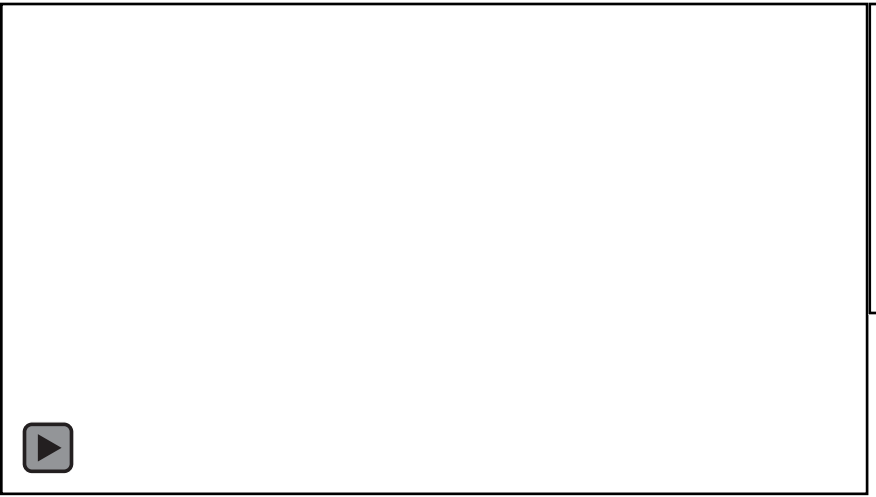
- ICON Beam line of SINQ largest aperture 80mm, Neutron flux: 2e8 n/cm^2/s
- space resolution ~0.5mm (modest due to low L/D=95 and pixel binning to improve counting statistics)
- A 300-um thick, ^{6}LiF/ZnS(Cu) scintillator screen
- Hamamatsu ORCA Flash 4.0 high-speed sCMOS camera + 50mm NIKKOR 1:1.4 lens
- Max. imaging speed 800 fps
- Object: flat aluminum (2 mm wall) bubbler (5 mm air/water)

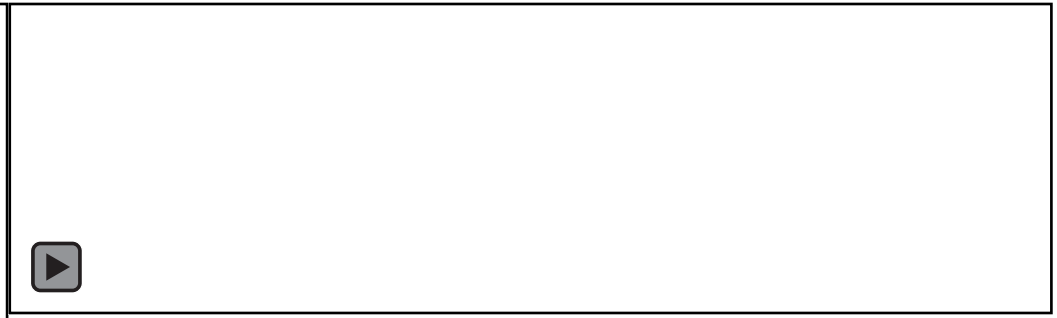


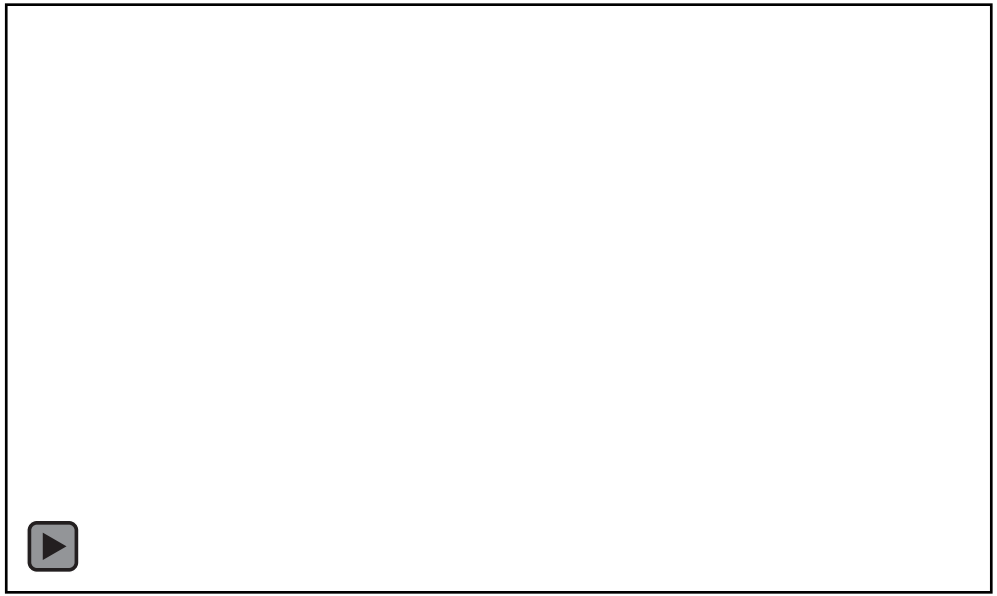


R. Zboray, P Tritk (2018)

High speed NI of two-phase flows in a bubbler



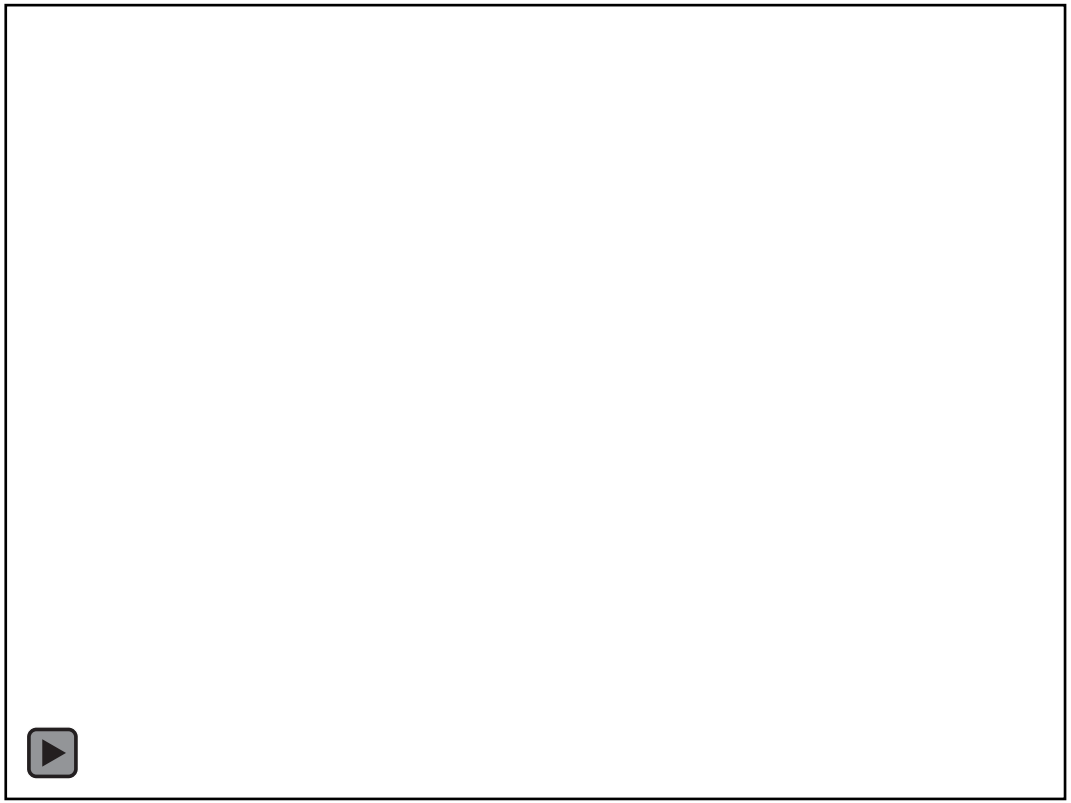




R. Zboray, P Tritk (2018)

TRIGA Reactor pulsing

TRIGA (Training, Research, Industry, General Atomic)



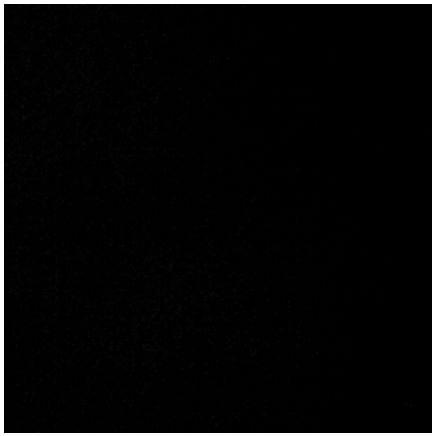
Breazeale reactor of Penn State University, source:
https://www.youtube.com/watch?v=6I3JKYdGWTE

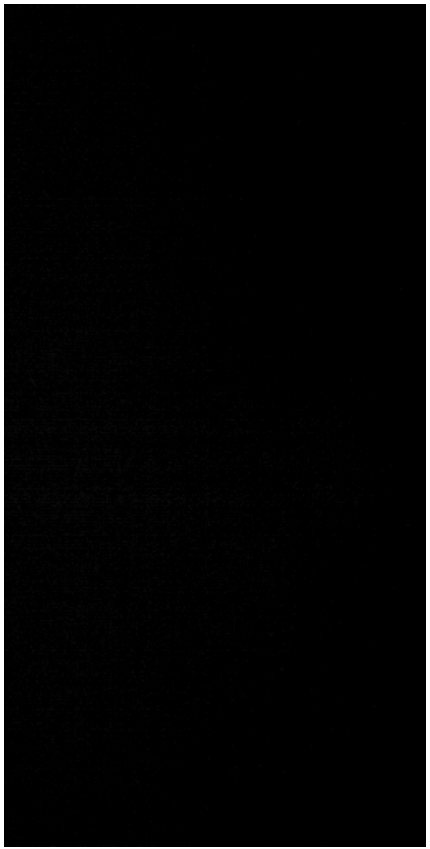
Bright flash neutron imaging @ 1MW Penn State Reactor

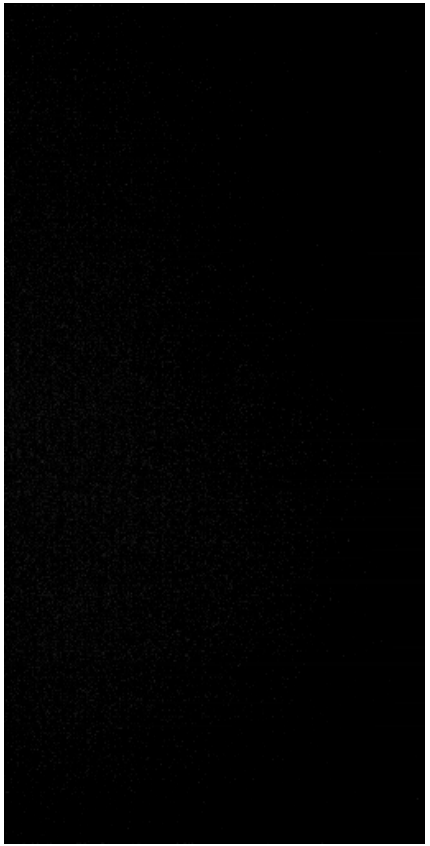
4000 fps for a 2.5$ pulse

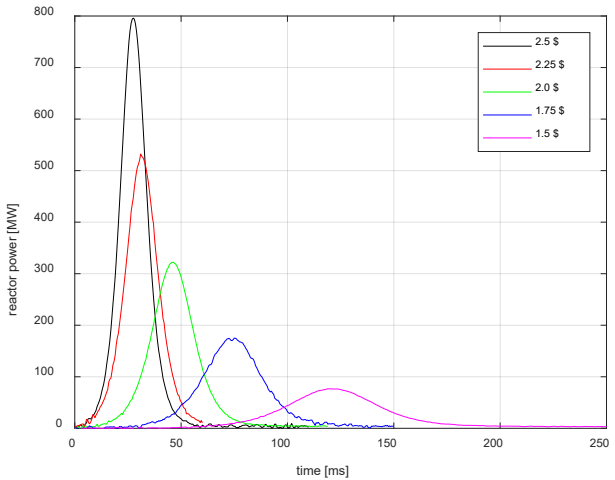
2000 fps for a 2.5$ pulse

2000 fps for a 2$ pulse









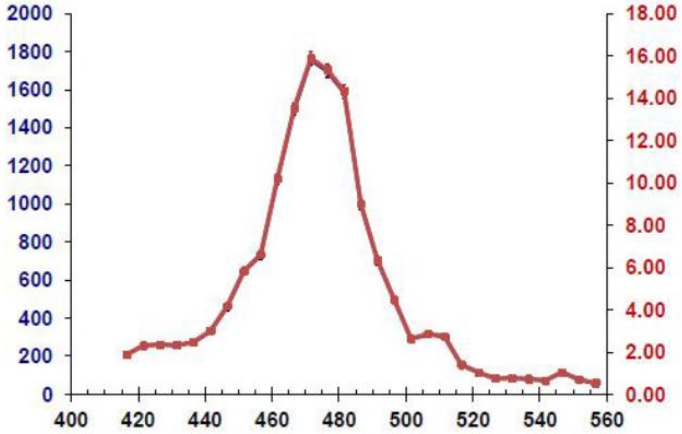
Gray scale is arbitrary

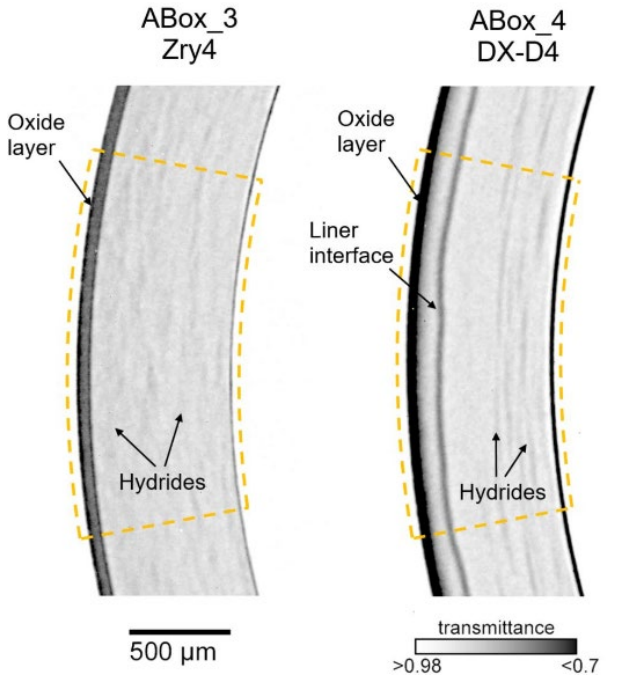
Ch. Lani & R. Zboray , NIM A (2020)

Hydration of Zr nuclear fuel cladding

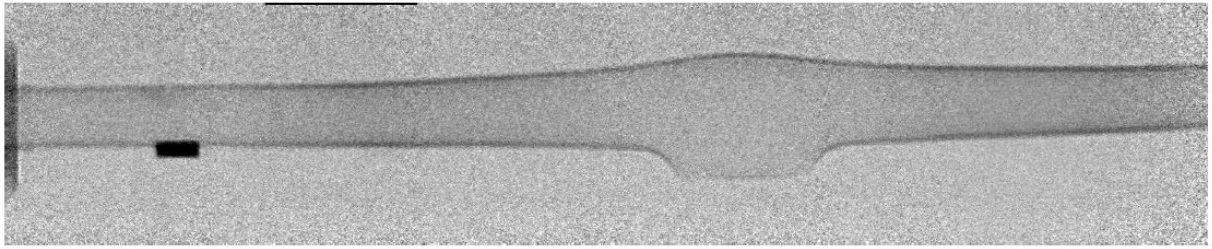






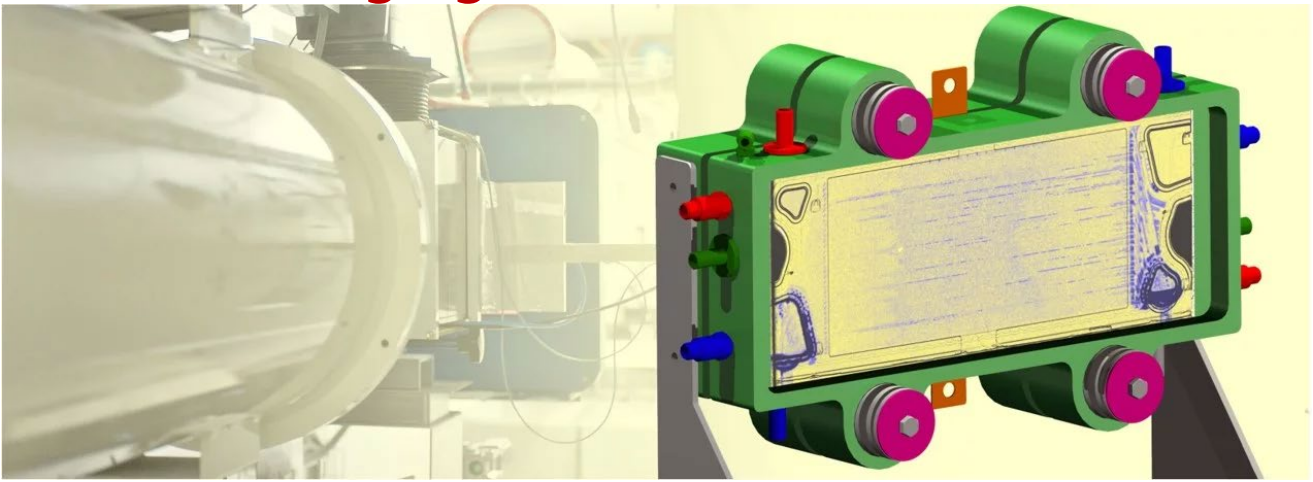


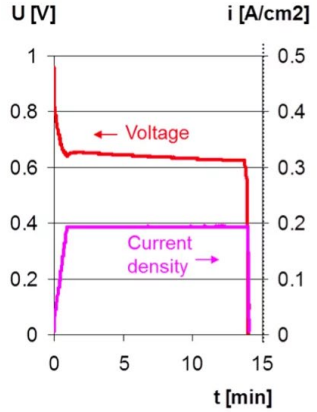
Duarte et al., 2021

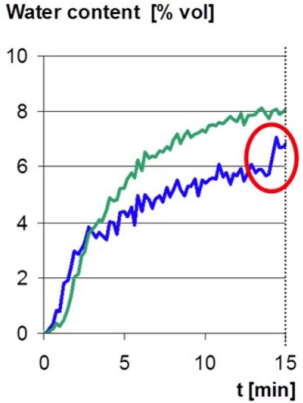


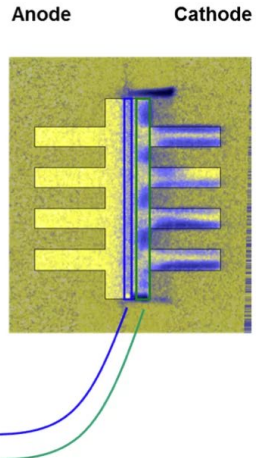
- Process leading accidental situation in NPPs: loss of coolant accident (LOCA)
- NR: H-distribution in Zr fuel rod cladding around the burst

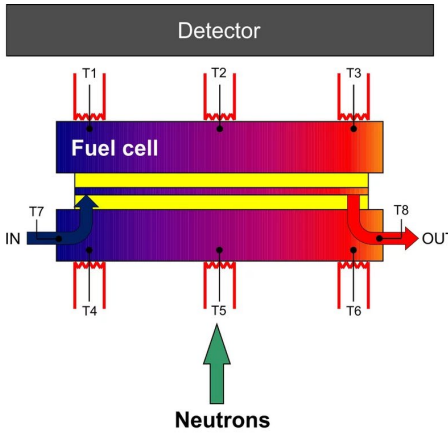
Neutron imaging of fuel cells

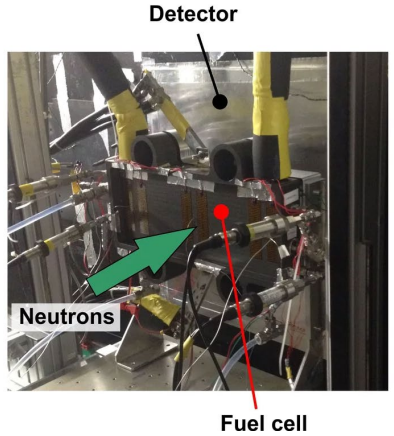






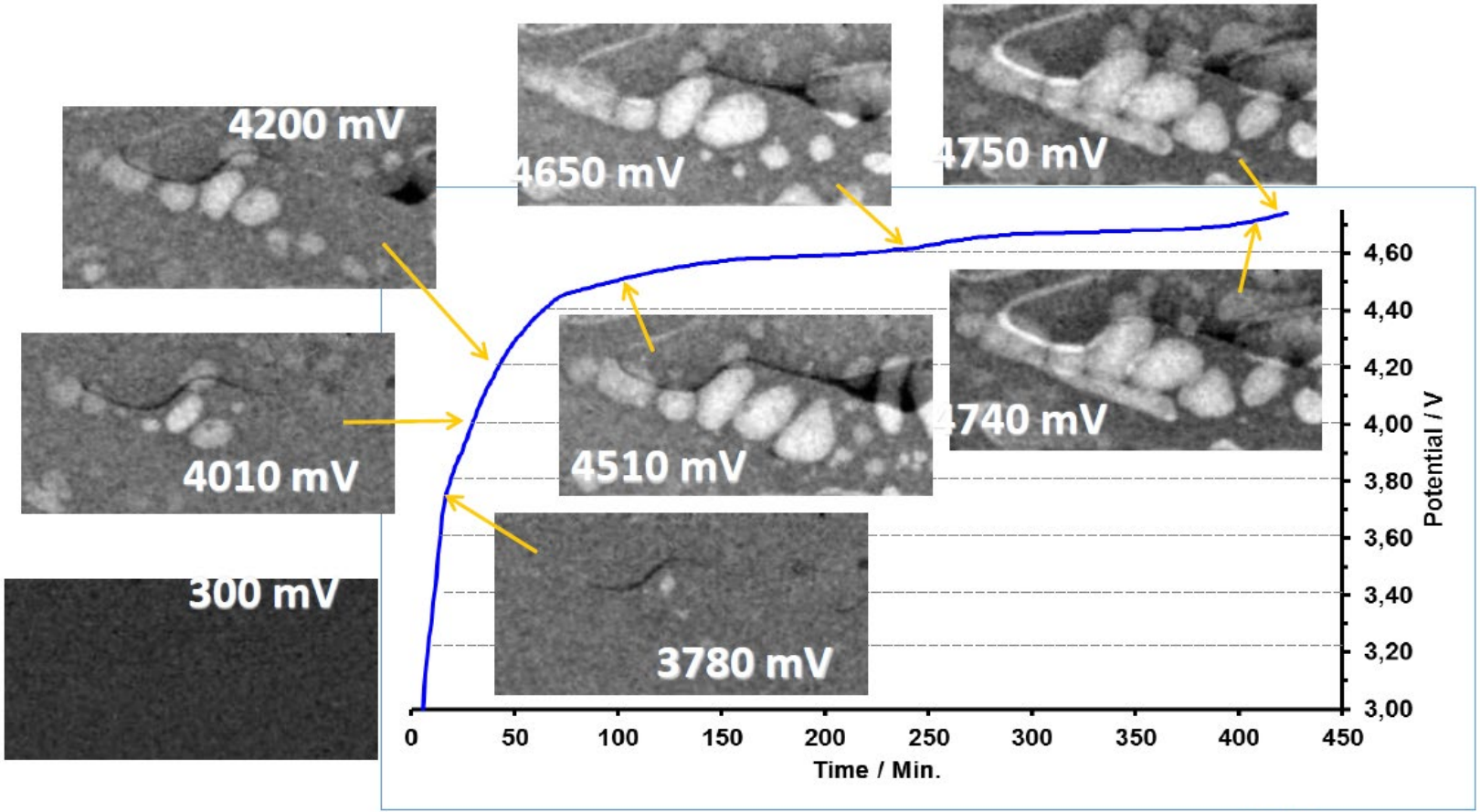






https://www.psi.ch/en/lec/projects/neutron-imaging-of-water-distribution-in-full-size-automotive-fuel-cells

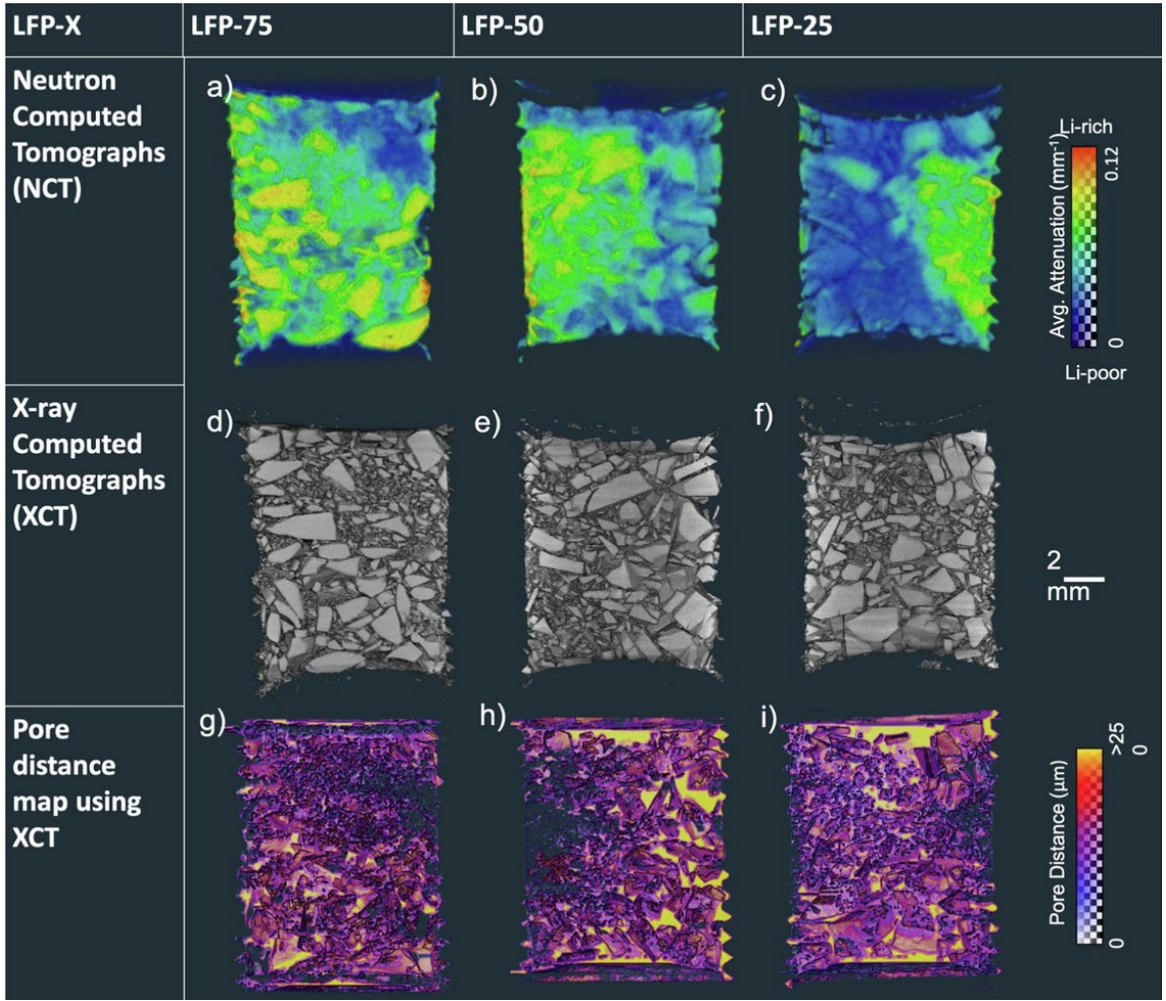
Gas formation during charge cycle of Li-Ion battery



H. Sommer

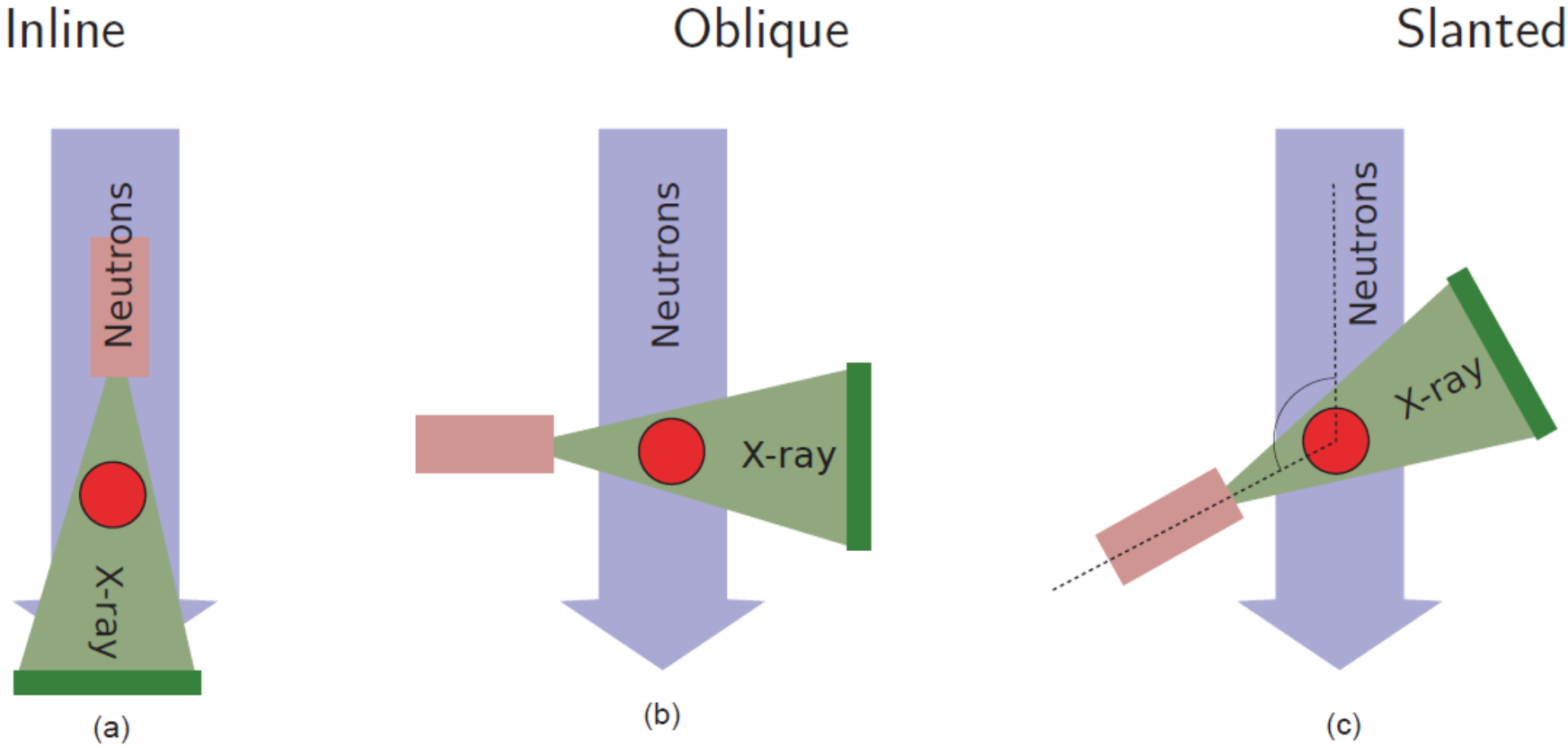
Chemical oxidation of lithium-ion cathode material in a packed bed reactor

Gupta et al., 2023



Bimodal Neutron/X-ray imaging applications

Geometries for bimodal thermal neutrons/X-ray imaging



Bimodal neutrons/X-ray imaging cultural heritage

Study of the inner content of Buddha sculptures (photo: example of Sakyamuni, Bhumisparsa Mudra, West-Tibet, 14.- 15. century):

X-rays



X-ray show no internal content

Bronze Buddha



NIAG PSI, https://www.psi.ch/niag/cultural-heritage

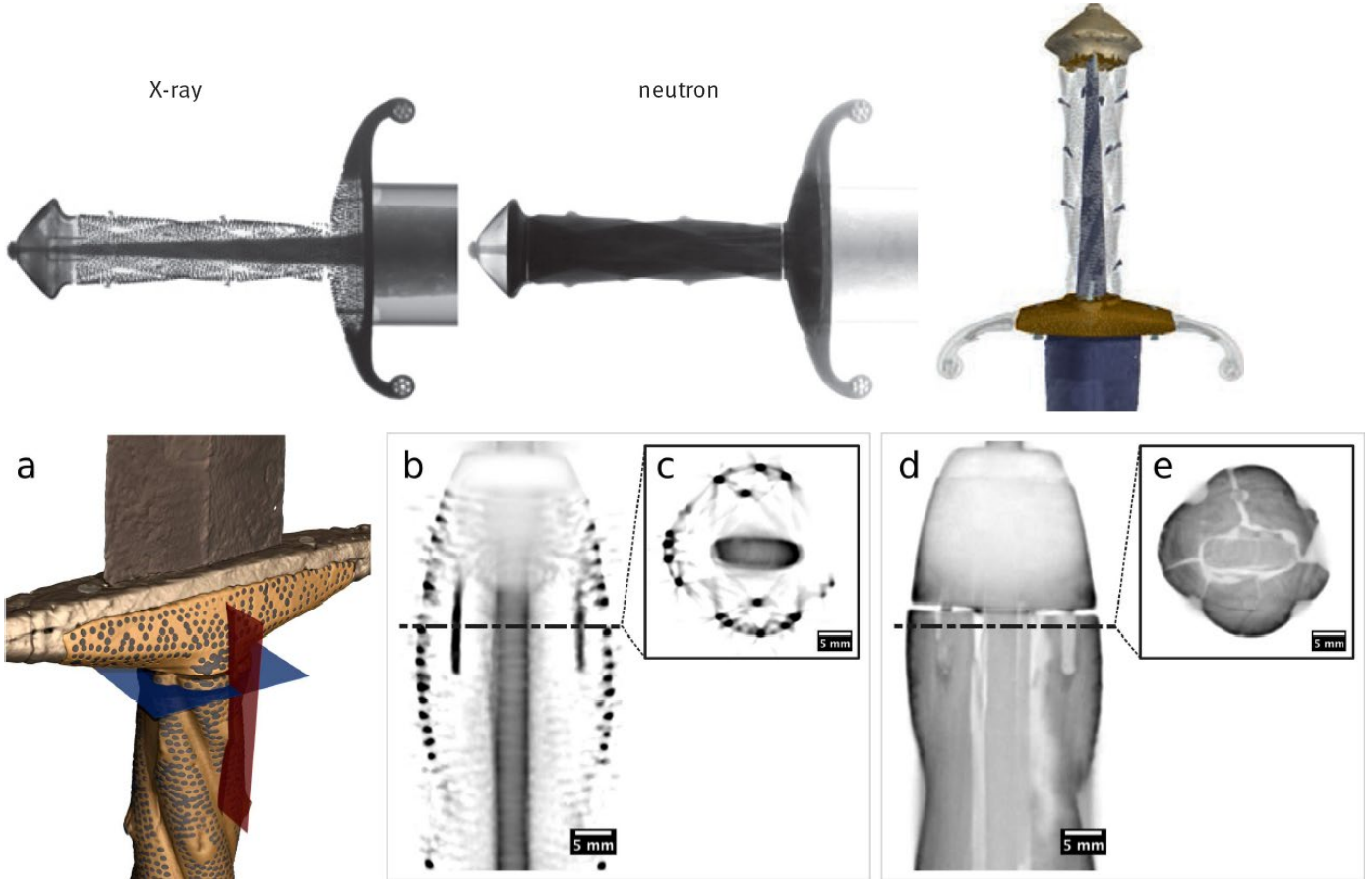
Neutronen



Neutrons reveal embedded organic material

Bimodal neutrons/X-ray imaging cultural heritage

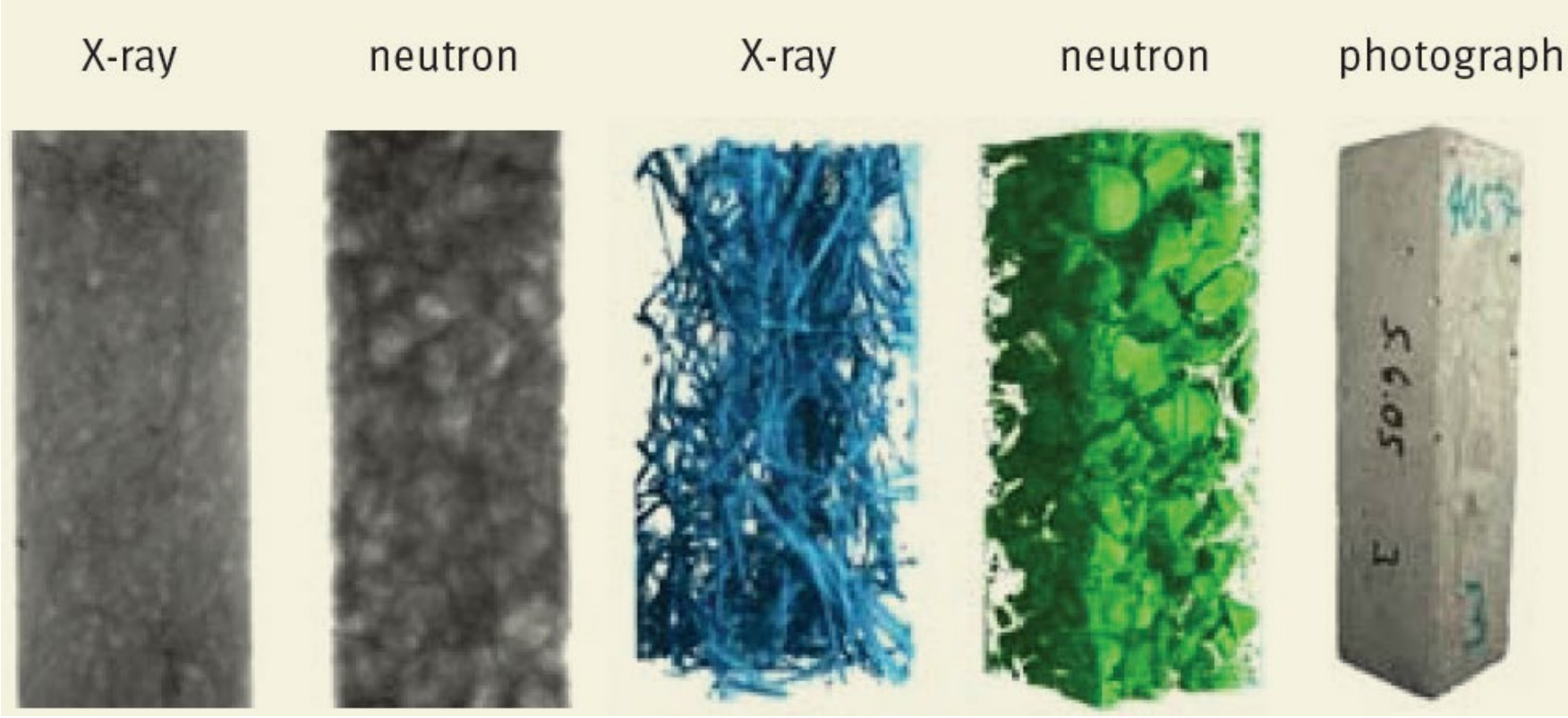
Radiographs and tomographic reconstruction of a wooden sword grip originating from the middle age. The combination of neutron and X-ray imaging reveals the inner shape of wooden parts and the rich metallic decoration:



NIAG PSI, https://www.psi.ch/niag/cultural-heritage

Bimodal neutrons/X-ray imaging of concrete

Bimodal imaging of a concrete sample embedded with steel fibers. The rendering of the neutron tomography volume in green shows clearly all components containing hydrogen e.g. cement, sand, but the embedded steel fibers are invisible. Displayed in blue, the X-ray CT of the same sample shows the embedded steel fibers.



Bimodal neutrons/X-ray imaging of plant-soil systems

Plant root water uptake: solid sample with a small Lupin plant -> roots highlighted by neutrons, denser stones by X-rays

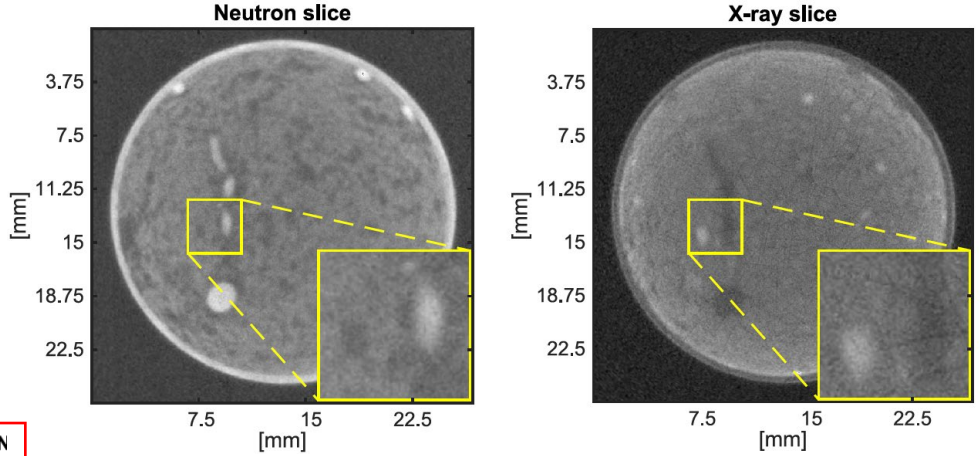
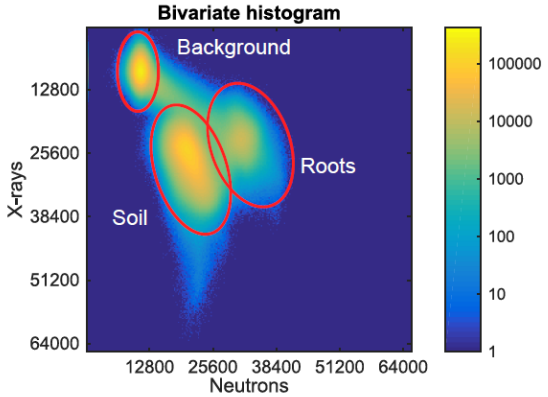
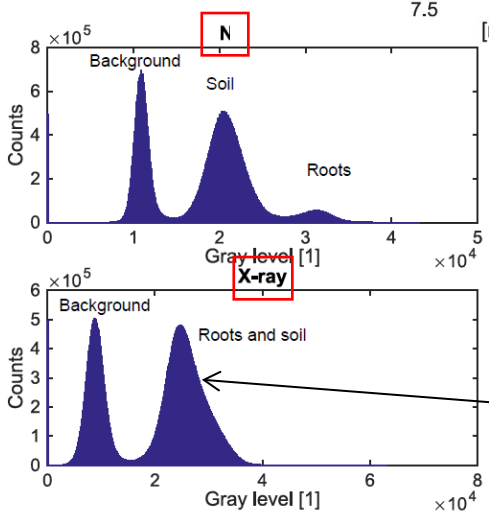


Image segmentation:
based on bivariate histogram





Separated histograms

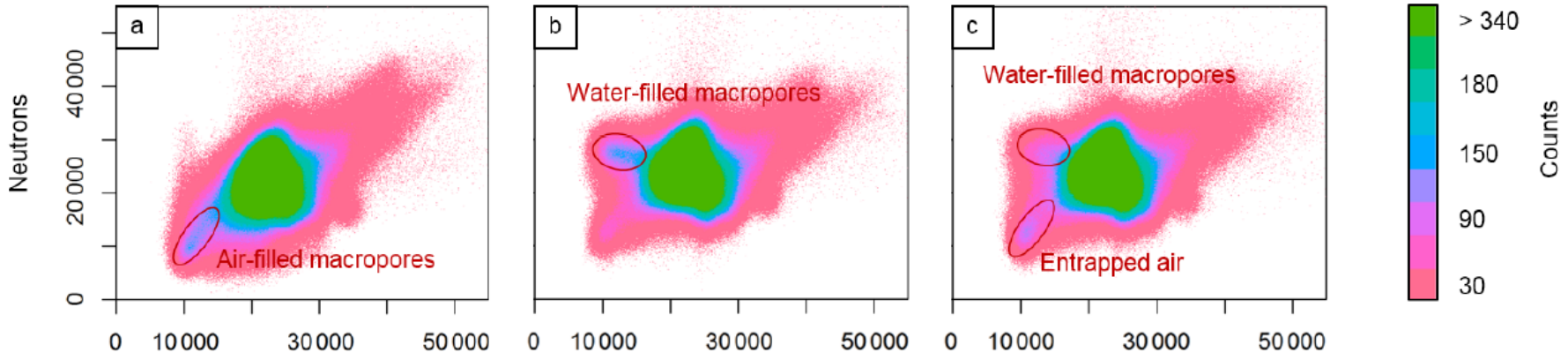
Solid and roots overlap

Kaestner et al., Bimodal Neutron/X-ray Imaging, DIR2015, Ghent, June 2015

Bimodal neutrons/X-ray imaging of concrete

Study of water and air behavior in soil: infiltration of water and trapping of air in coarse loam soil.

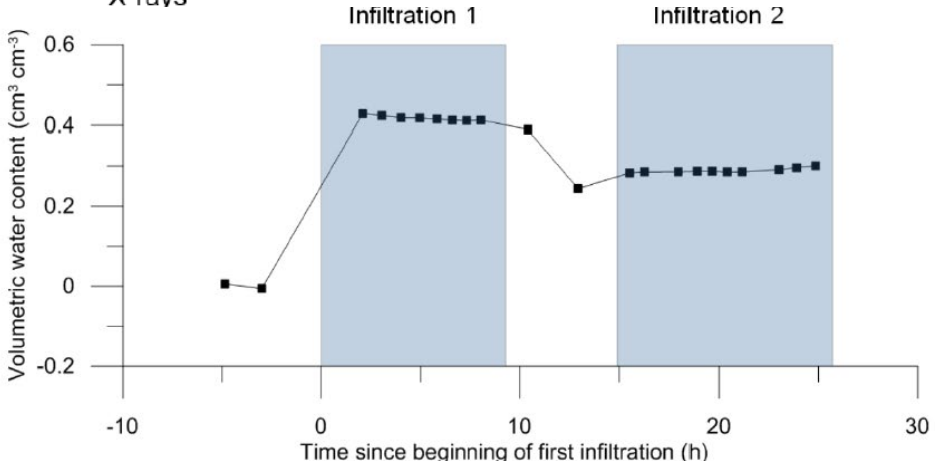
Image segmentation: based on bivariate histogram



Macropore: X-ray image segmentation



Water content by neutrons:
using D2O+H2O mixture

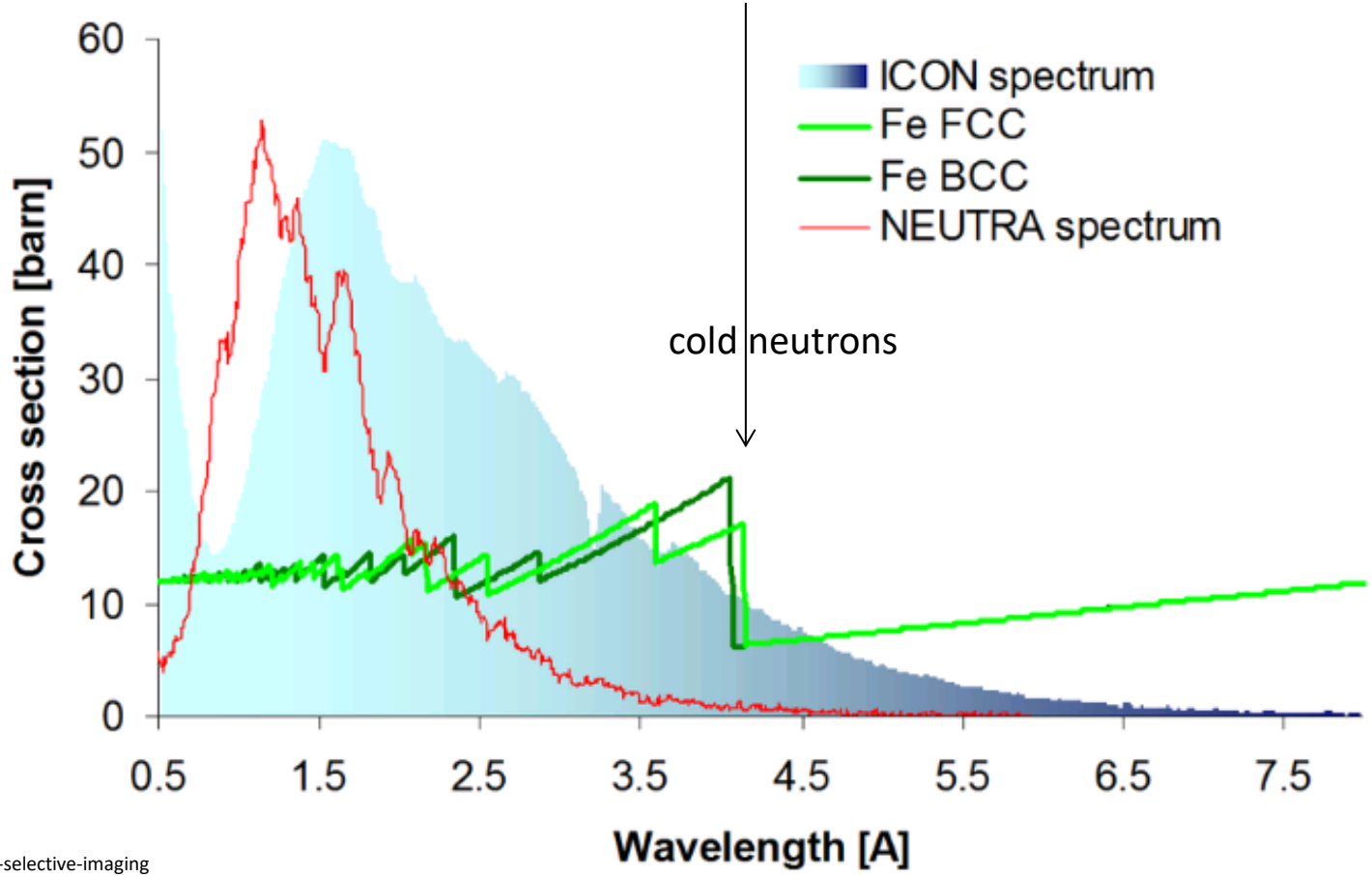


Kaestner et al., Solid Earth (201/)

Energy-selective neutron imaging applications

Energy-selective cold/thermal neutron imaging

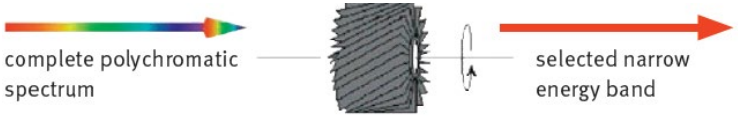
Investigating materials with crystal lattice structure (showing Bragg edges):

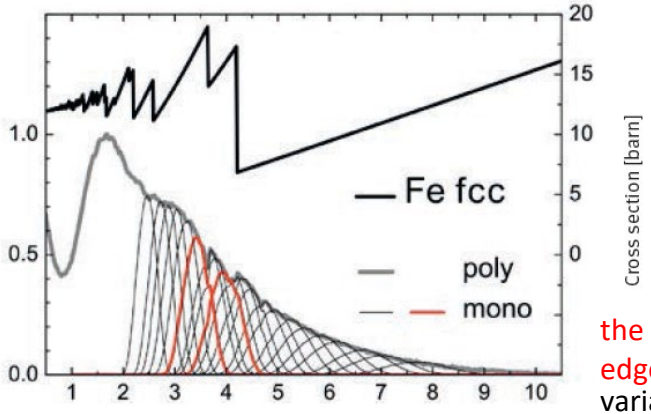


https://www.psi.ch/niag/energy-selective-imaging

Energy-selective cold/thermal neutron imaging

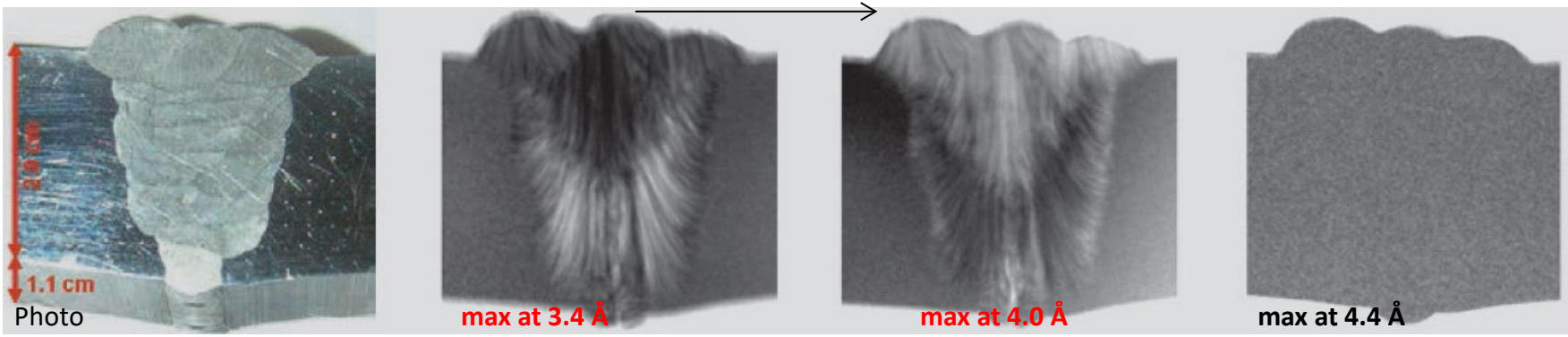
Studying a thick **steel weld joint** using quasi mono-energetic (narrow wavelength band) beams:





Neutron Imaging Leaflet, NIAG PSI,
https://www.psi.ch/niag/ImagingBrochureEN/Neutron_Imaging_m3.pdf

the narrow energy band must overlap with a Bragg edge to enhance crystal structure in image variations in crystal lattice properties



Neutron Bragg edge tomography

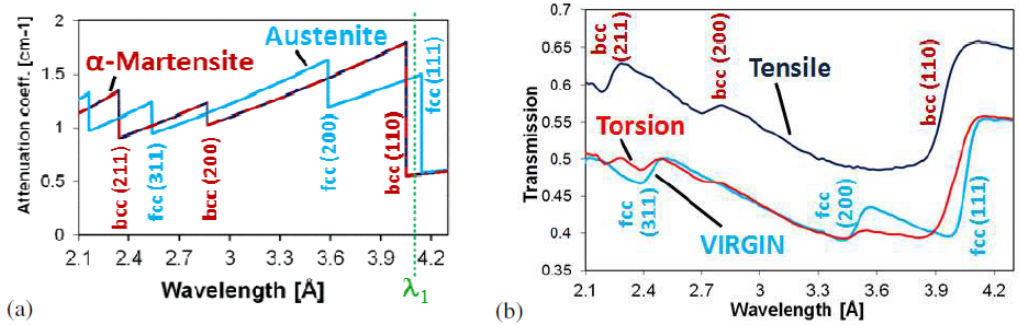


Fig. 2. (a) Theoretical Bragg edge spectra for the Austenite and α-Martensite phases of iron. The depicted wavelength λ_1 will yield a distinct contrast between the two phases. (b) Bragg edge transmission spectra for three different samples: The undeformed sample (VIRGIN) shows only Bragg edges corresponding to the Austenitic phase, while the middle of the tensile sample shows only Bragg edges corresponding to the Martensitic phase. The middle of torsion sample shows Bragg edges corresponding to both phases due to the nature of the strain distribution.

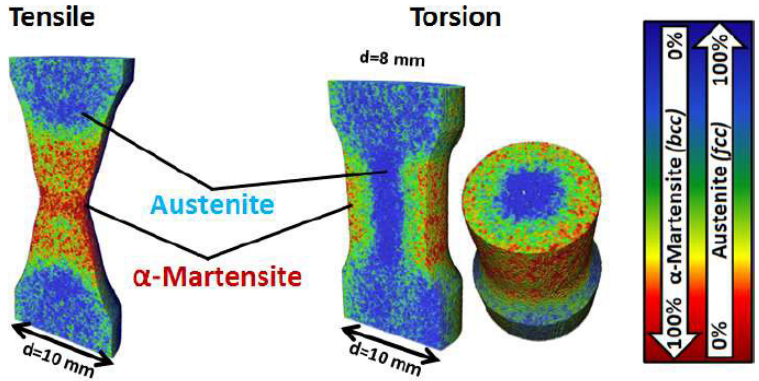


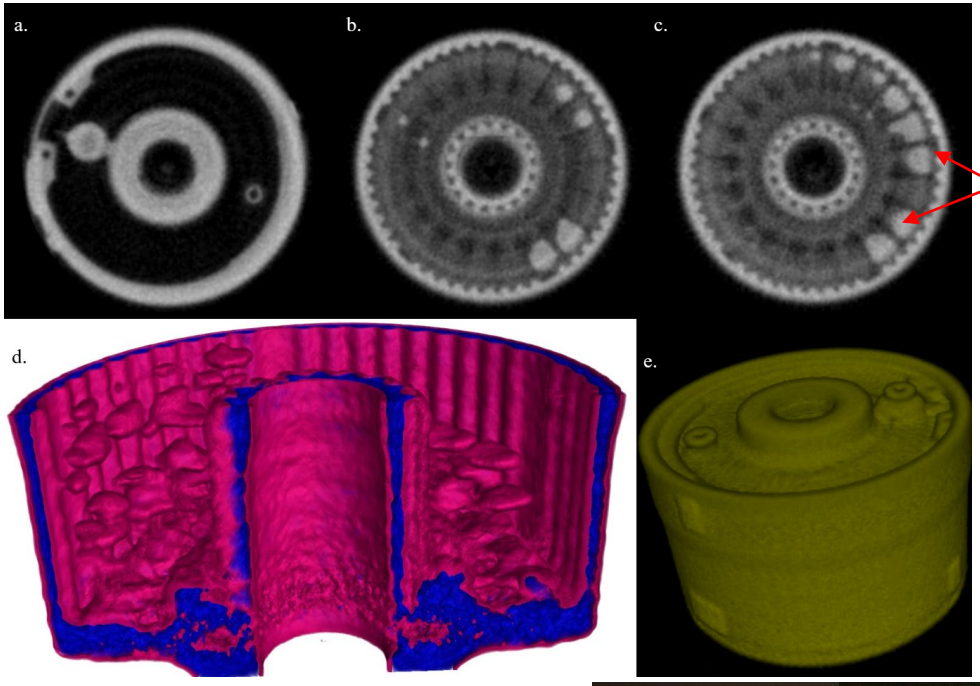
Fig. 3. Tomographic reconstruction of the phase fractions for the tensile and torsion sample. The necking region of the tensile sample is fully transformed to Martensite. The radial dependence of the phase transformation in the torsion sample is revealed and quantified.

Woracek et al., Phys Proc. (2015)

Applications of fast neutron imaging

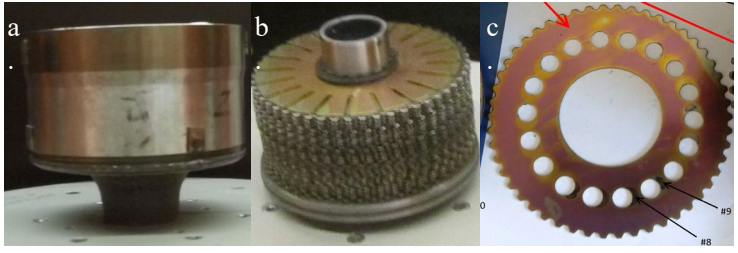
Fast neutron imaging at RAD @ BNC

Imaging of a viscous coupling (chopper) Ø 15cm massive metal structure with rest oil inside



Oil droplets between the discs

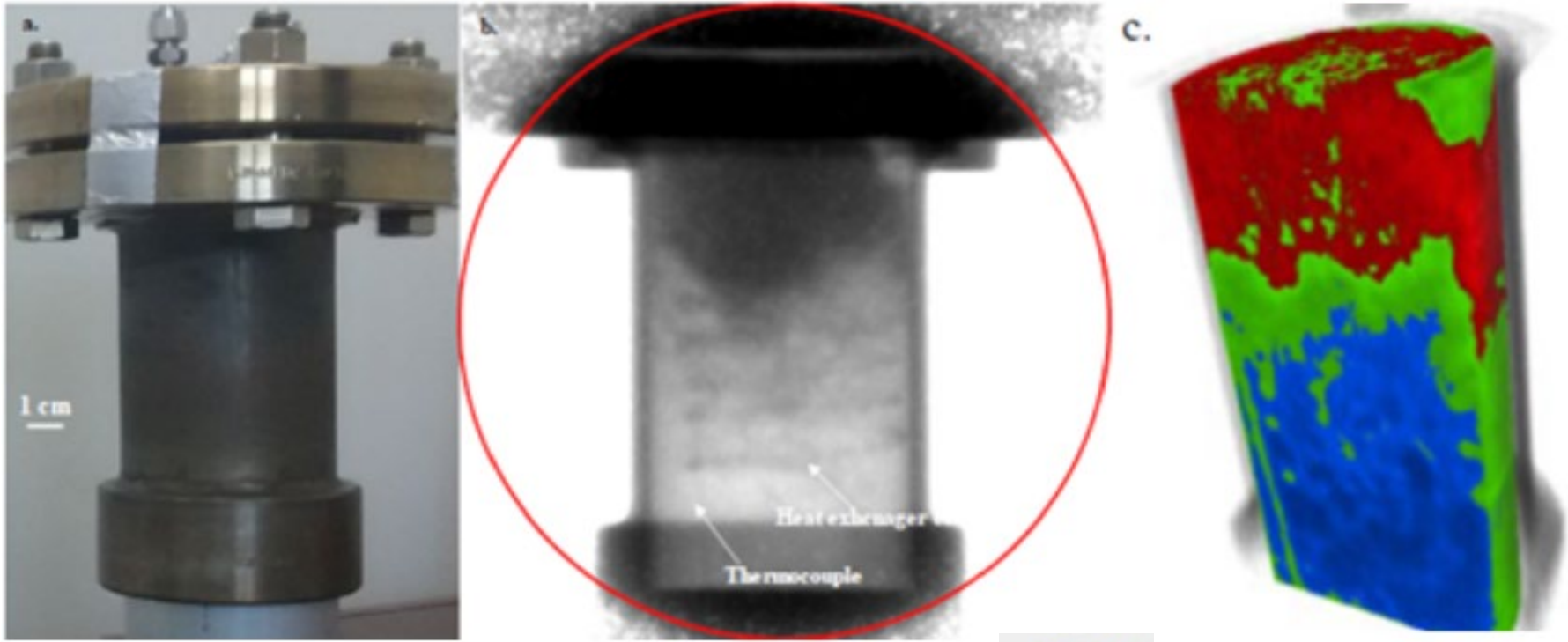
Works for large and/or very attenuating objects!



Zboray et al., AppRad (2017)

Fast neutron imaging at RAD @ BNC

Li-fueled reactor for powering planetary landers. The device reacts stored lithium fuel with readily accessible in situ oxidizers on planetary surfaces such as Mars

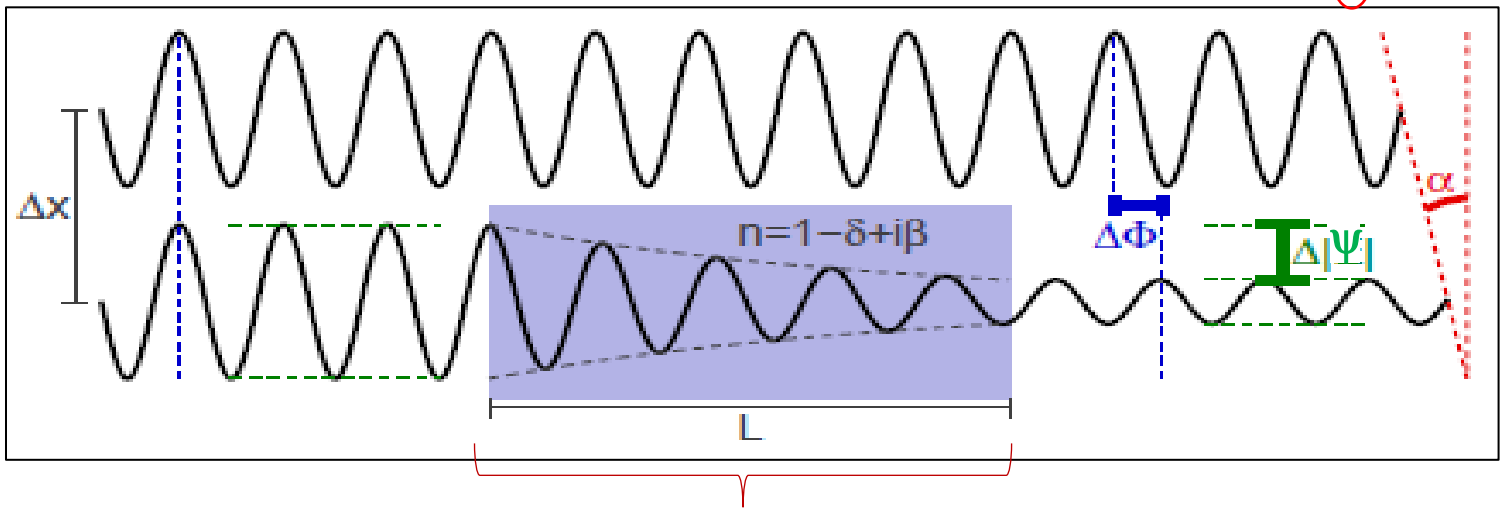


Zboray et al, WCNR 11, 2018

Alternative imaging modalities

Wave characteristic of X-rays, index of refraction

Wave propagation in media with complex index of refraction: $n(\omega) = 1 - \delta + i\beta$



k- wave number

λ- wave length

$$k = \frac{2\pi}{\lambda}$$

Refraction angle:

$$\alpha = \frac{\Delta\Phi/k}{\Delta x}$$

f - frequency

ω- angular frequency

$$\omega = 2\pi f$$

plane wave function

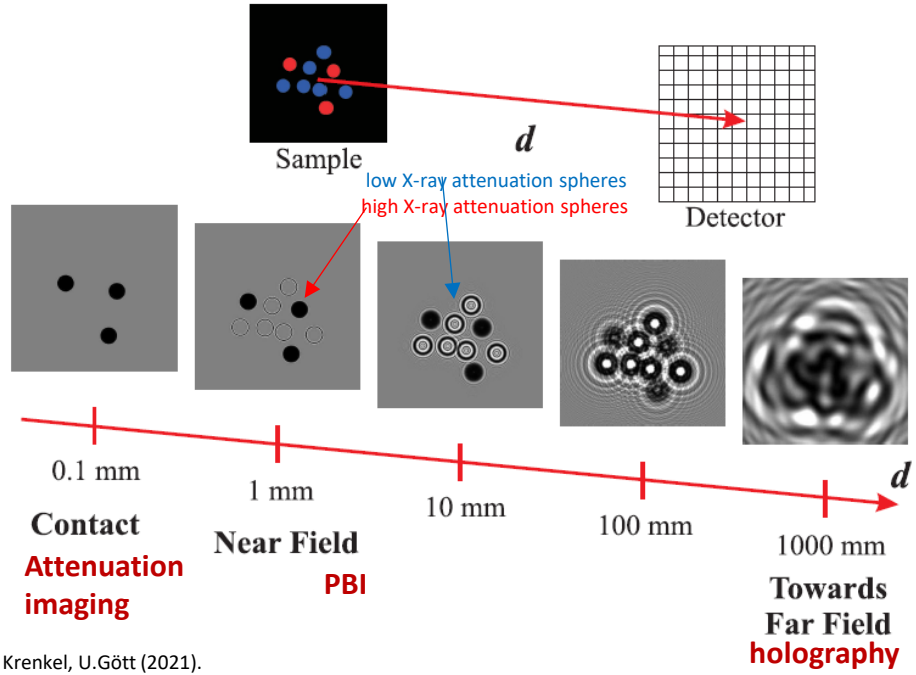
$$\Psi_m(z,t) = \Psi_0\, e^{i(nkz-\omega t)} = \Psi_0\, e^{-i\omega t}\, e^{(1-\delta)ikz}\, e^{-\beta kz}$$

$$= \Psi_v(z,t) \cdot \underbrace{e^{-i\delta kz}}_{\text{Phase shift}} \cdot \underbrace{e^{-\beta kz}}_{\text{attenuation}}$$

Intensity~$|\psi|^2$

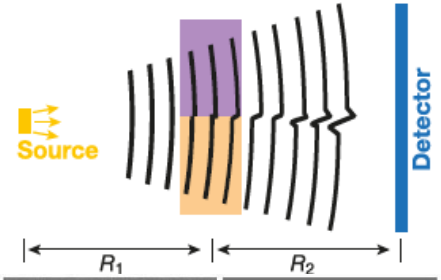
Phase contrast imaging (PCI) by propagation

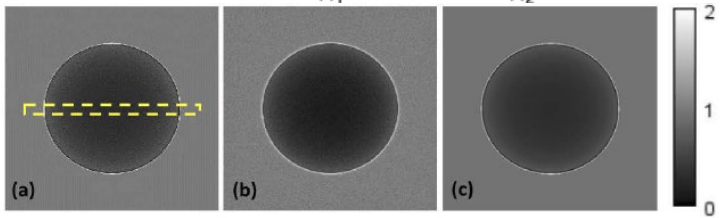
Phase contrast effects get emphasized by free-space propagation behind the sample:

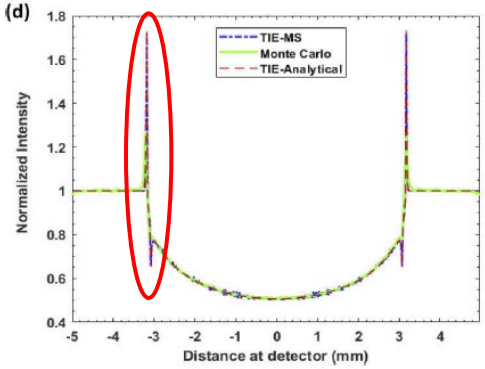


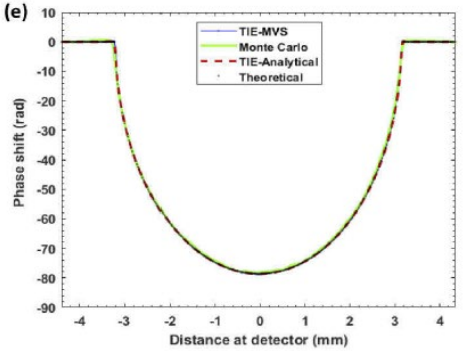
Krenkel, U.Gött (2021).

Edge enhancement:





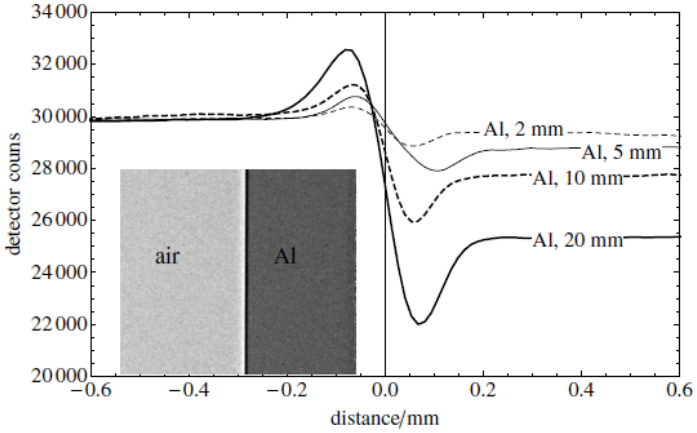


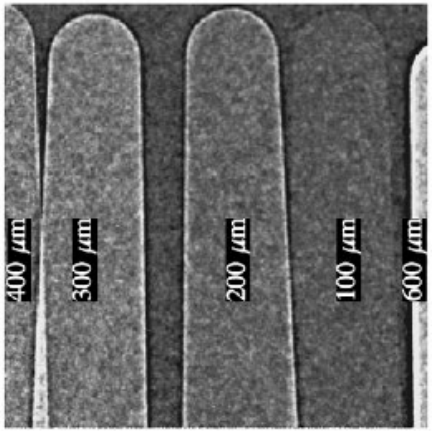


Saghamanesh & Zboray, Opt Exp. (2021).

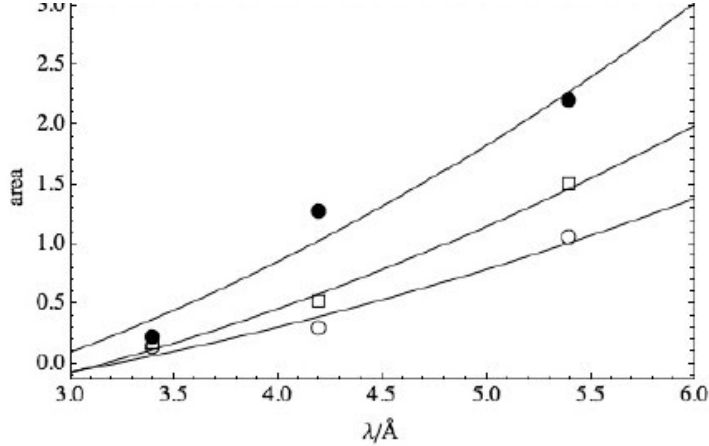
Edge enhancement in the near field is used!

Phase contrast imaging with neutrons





(a) image



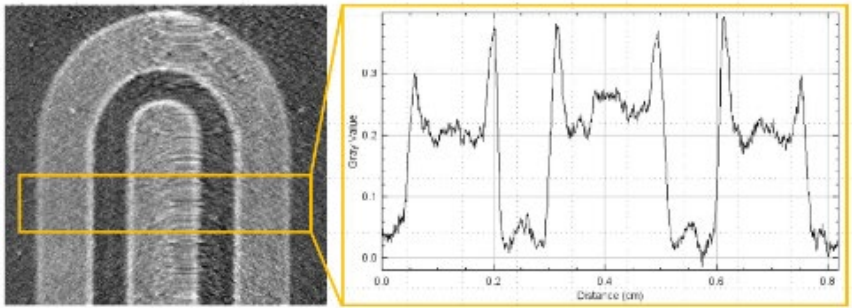
(b) fit

Butler & Lehmann, 2013

$$n = \sqrt{1 - \frac{V}{E}} = 1 - \delta_{nuc} - \delta_{mag} + i\beta$$

$$\beta = \frac{\sigma_r N \lambda}{4\pi} \quad \delta_{nuc} = \frac{\lambda^2 N b_c}{2\pi} \quad \delta_{mag} = \pm\frac{\boldsymbol{\mu}_N \cdot \boldsymbol{B}}{2E_0} = \pm\frac{2\boldsymbol{\mu}_N \cdot \boldsymbol{B} m \lambda^2}{h^2}$$

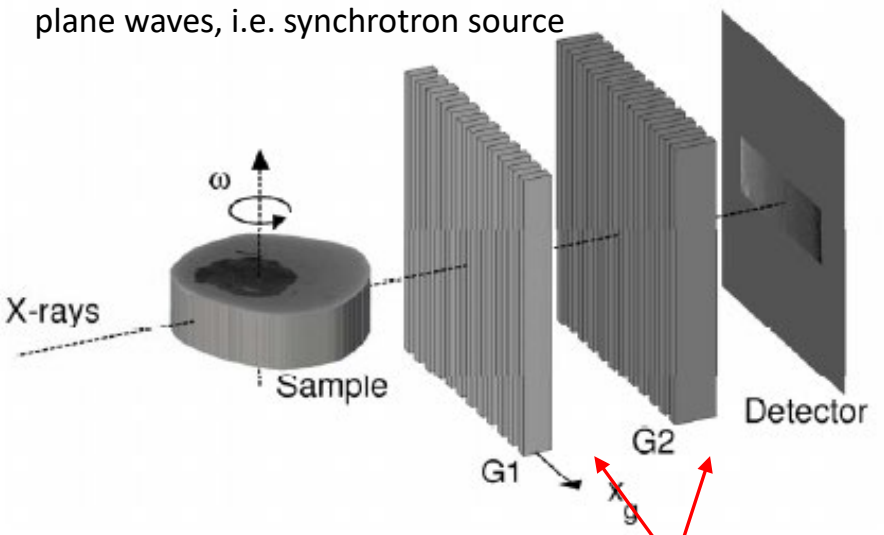
the material density N and the coherent scattering length b_c



BNC NORMA unpublished

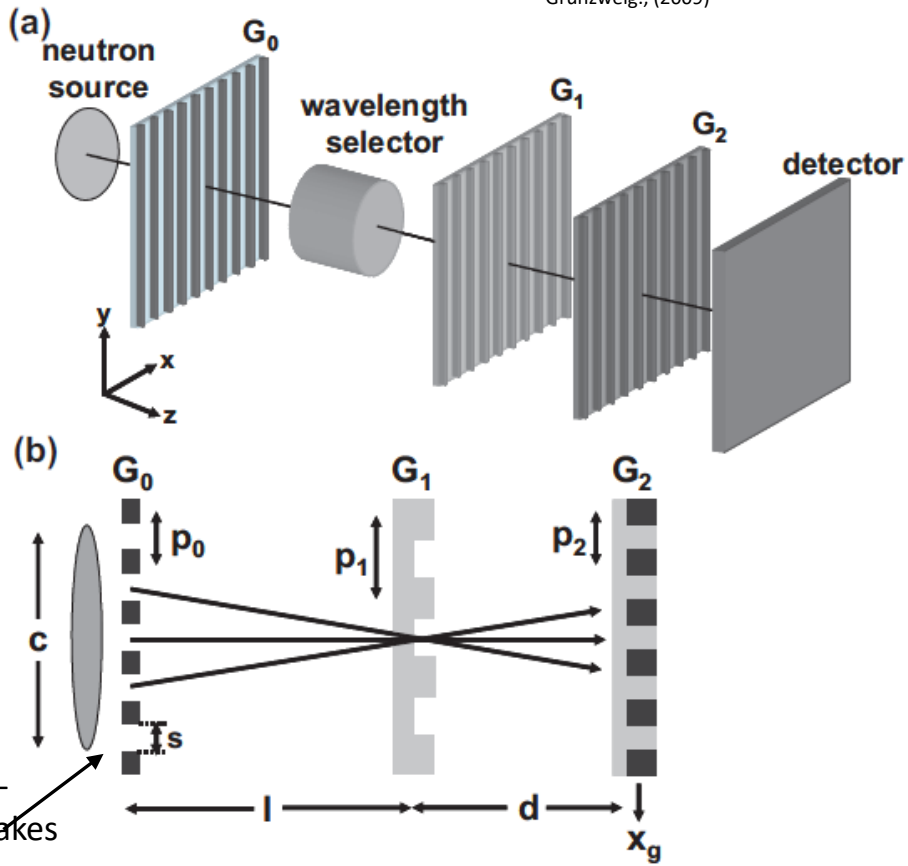
Gratings-based PCI/DFI methods

At perfectly parallel beam of monochromatic plane waves, i.e. synchrotron source



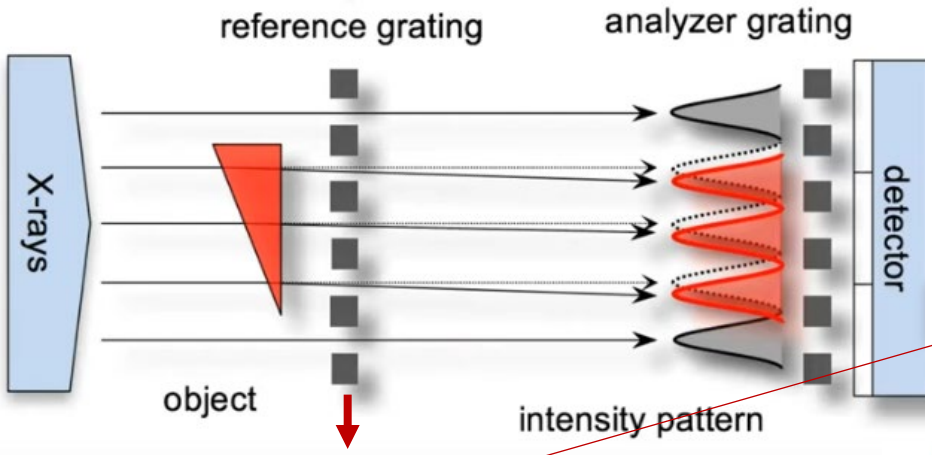
Talbot-Lau interferometer: interference pattern is created between G1 & G2

Grünzweig., (2009)



At a non-coherent source (divergent, non-coherent, broad energy spectrum) - G0 makes the radiation partially coherent!

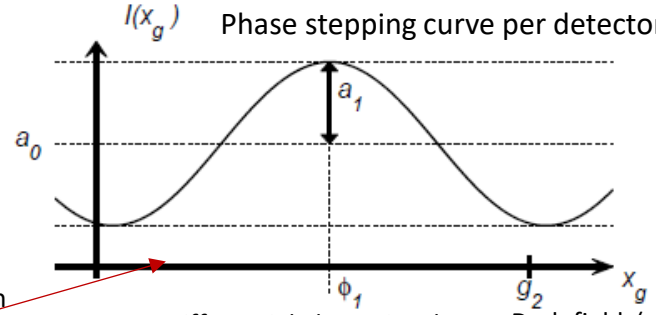
Gratings-based neutron PCI/DFI methods



E.g. G1 is shifted in very small steps to measure intensity modulation curve on detector over a grating period

This is done without (r) and then with the sample (s) in place!

Phase stepping curve per detector pixel:



Transmission (attenuation) signal:

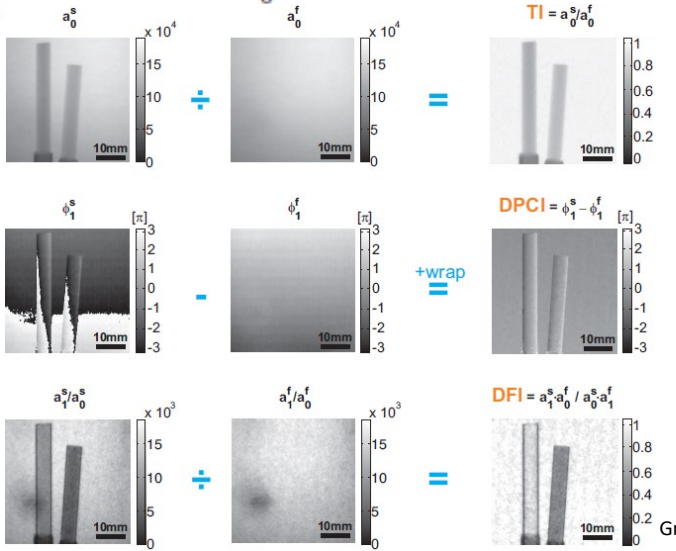
$$T(x,z) = \frac{a_0^{(s)}}{a_0^{(r)}}$$

Differential phase signal:

$$\phi_{1,s} - \phi_{1,r}$$

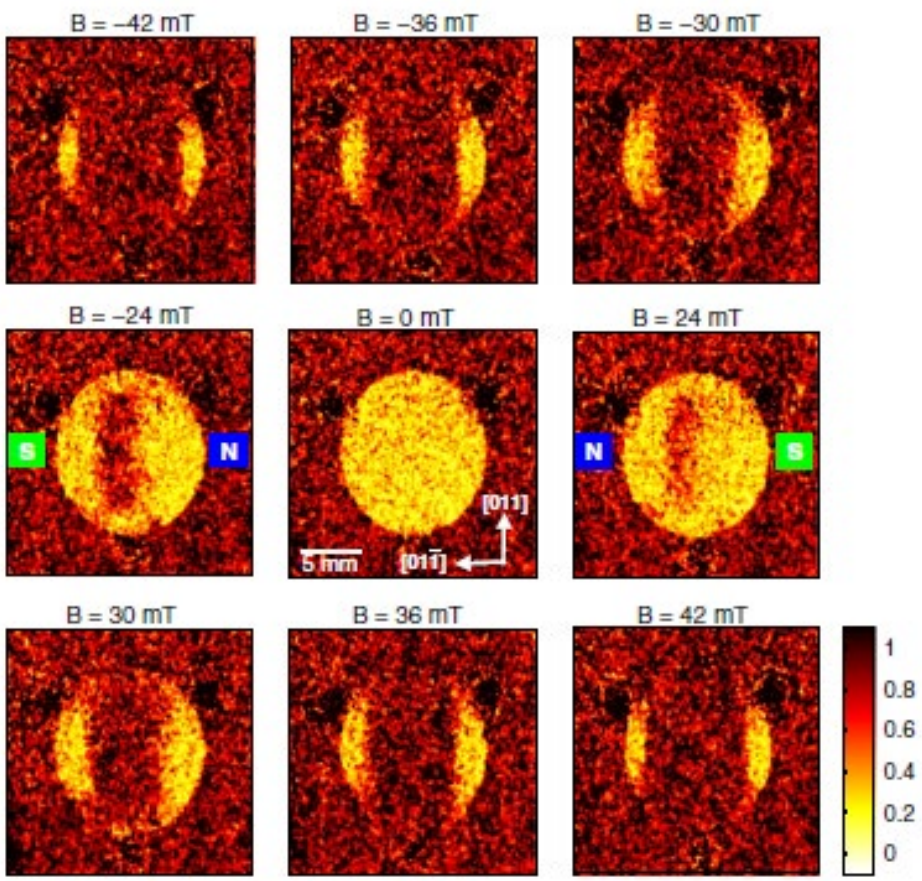
Dark-field (visibility) signal:

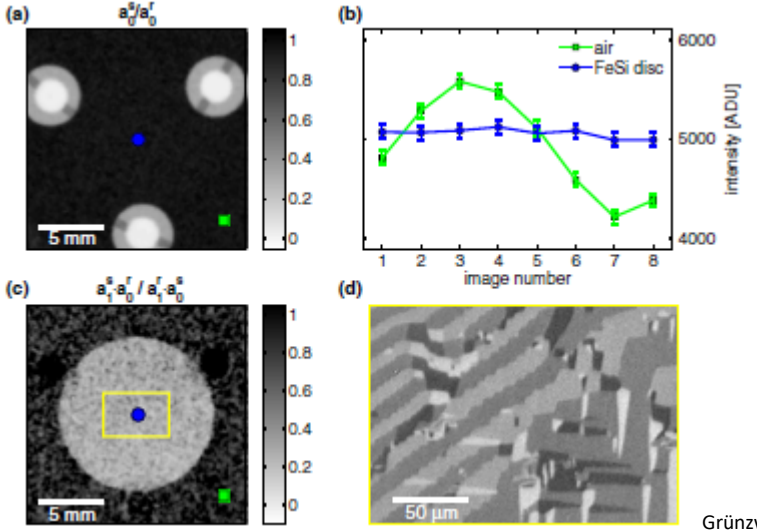
$$V(x,z) \equiv \frac{a_1^{(s)}/a_0^{(s)}}{a_1^{(r)}/a_0^{(r)}}$$



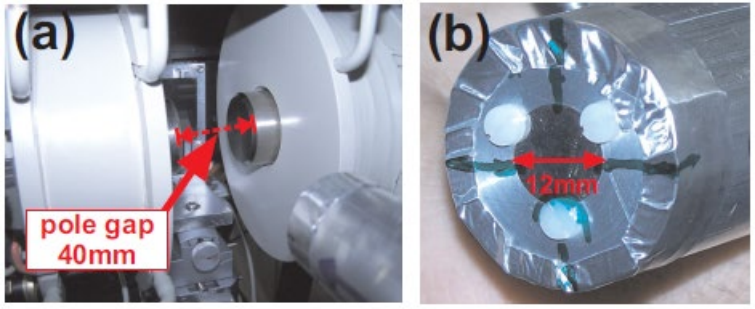
Grünzweig., (2009)

Studying magnetic domains by neutron DFI methods

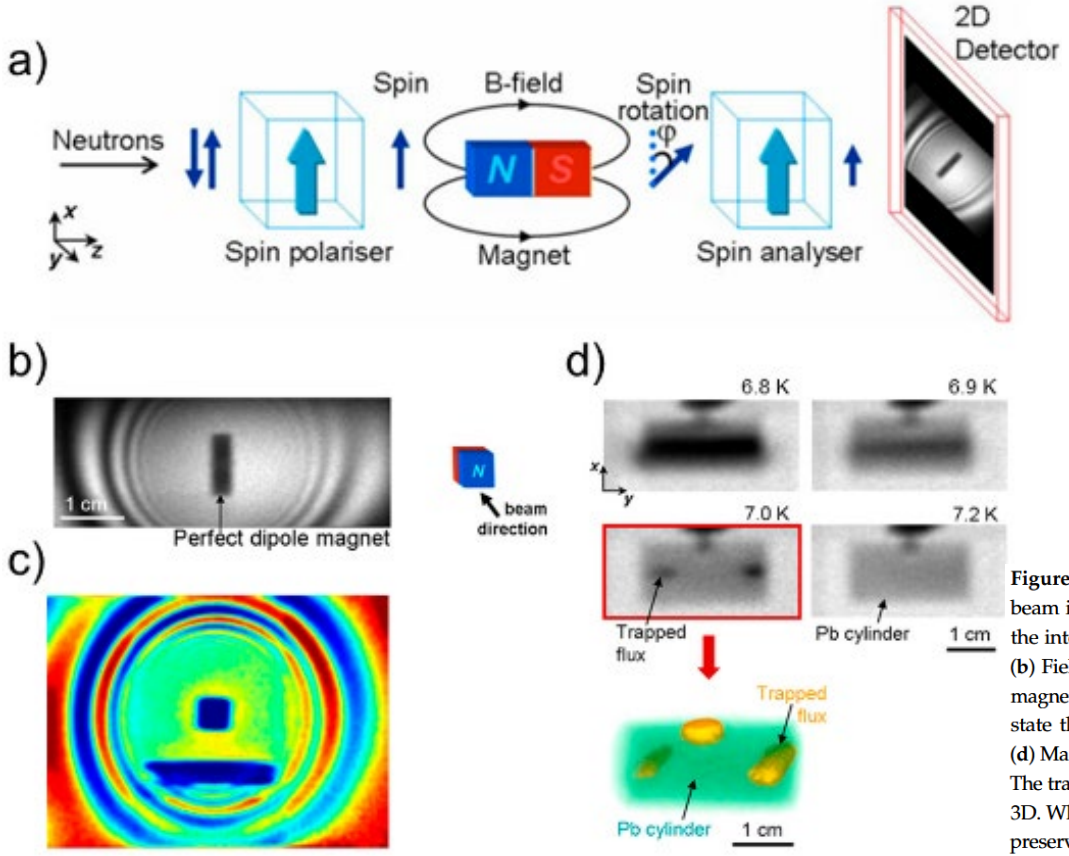




Grünzweig et al., (2008)



Magnetic field/domains by polarized neutron imaging



$$I(x,y) = \underbrace{I_0(x,y)\cdot\exp\left(-\int_{\text{path}}\Sigma(s)\mathrm{d}s\right)}_{I_a(x,y)}\cdot\underbrace{\frac{1}{2}\left(1+\cos\varphi(x,y)\right)}_{I_m(x,y)}$$

$$\frac{\mathrm{d}}{\mathrm{d}t}S_\alpha(t) = \frac{g\mu_\mathrm{N}}{\hbar}\left[\mathbf{S}(t)\times\mathbf{B}(t)\right]_\alpha$$

$$\omega_\mathrm{L} = \frac{g\mu_\mathrm{N}}{\hbar}B = \gamma_\mathrm{L}B$$

γ_L is the gyromagnetic ratio
μ_N is the nuclear magneton

Figure 1. **(a)** Schematic diagram of a set-up used for imaging magnetic materials and fields. The neutron beam is polarized, then precesses in a magnetic field, eventually is analyzed and detected. Note that the intensity (dark blue arrow) behind the analyzer is smaller than the intensity behind the polarizer; **(b)** Field lines surrounding a simple dipole magnet; **(c)** Radiograph showing field lines around a bar magnet levitating over an yttrium-barium-copper-oxide (YBCO) superconductor as in its superconducting state the YBCO expels all magnetic fields and thus repels the permanent magnet (Meissner effect); **(d)** Magnetic field trapped in a polycrystalline lead cylinder at different temperatures around T_c = 7.2 K. The trapped flux (yellow regions left and right) inside a polycrystalline cylinder of lead is reconstructed in 3D. When cooled to below its critical temperature in the presence of a weak magnetic field some flux is preserved inside the sample due to defects and grain boundaries and this remains trapped even after the field is switched off [2].

Kardjilov et al., (2008, 2018)

Thank you for your attention!



